Mon. Not. R. Astron. Soc. **359,** 906–926 (2005) doi:10.1111/j.1365-2966.2005.08928.x

# A study of the Type II-P supernova 2003gd in M74

M. A. Hendry,[1⋆] S. J. Smartt,[2] J. R. Maund,[1] A. Pastorello,[3] L. Zampieri,[4] S. Benetti,[4] M. Turatto,[4] E. Cappellaro,[5] W. P. S. Meikle,[6] R. Kotak,[6] M. J. Irwin,[1] P. G. Jonker,[7] L. Vermaas,[8] R. F. Peletier,[8] H. van Woerden,[8] K. M. Exter,[9] D. L. Pollacco,[10] S. Leon,[11] S. Verley,[11] C. R. Benn[12] and G. Pignata[4,13]

[1]*Institute of Astronomy, University of Cambridge, Madingley Road, Cambridge CB3 0HA*
[2]*Department of Physics and Astronomy, Queen's University Belfast, Belfast BT7 1NN*
[3]*INAF – Osservatorio Astrofisico di Arcetri, Largo E. Fermi 5, I-50125 Firenze, Italy*
[4]*INAF – Osservatorio Astronomico di Padova, Vicolo dell' Osservatorio 5, I-35122 Padova, Italy*
[5]*INAF – Osservatorio Astronomico di Capodimonte, Via Moiariello 16, I-80131 Napoli, Italy*
[6]*Astrophysics Group, Blackett Laboratory, Imperial College London, Prince Consort Road, London SW7 2BZ*
[7]*Harvard-Smithsonian Center for Astrophysics, Cambridge, MA 02138, USA*
[8]*Kapteyn Instituut, Postbus 800, 9700 AV Groningen, the Netherlands*
[9]*Instituto de Astrofísica de Canarias, C/Vía Láctea s/n, E38200 La Laguna (Tenerife), Spain*
[10]*School of Pure and Applied Physics, Queen's University Belfast, Belfast BT7 9NN*
[11]*Instituto de Astrofísica de Andalucía (CSIC), Apartado 3004, 18080 Granada, Spain*
[12]*Isaac Newton Group, Apartado 321, E38700 Santa Cruz de La Palma, Spain*
[13]*European Southern Observatory (ESO), Karl-Schwarzschild-Str. 2, D-85748 Garching bei München, Germany*

Accepted 2005 February 12. Received 2004 November 29; in original form 2004 June 4

**ABSTRACT**

We present photometric and spectroscopic data of the Type II-P supernova (SN II-P) 2003gd, which was discovered in M74 close to the end of its plateau phase. SN 2003gd is the first Type II supernova (SN) to have a directly confirmed red supergiant (RSG) progenitor. We compare SN 2003gd to SN 1999em, a similar SN II-P, and estimate an explosion date of 2003 March 18. We determine a reddening towards the SN of $E(B-V) = 0.14 \pm 0.06$, using three different methods. We also calculate three new distances to M74 of $9.6 \pm 2.8$, $7.7 \pm 1.7$ and $9.6 \pm 2.2$ Mpc. The former was estimated using the standard candle method (SCM), for Type II supernovae (SNe II), and the latter two using the brightest supergiants method (BSM). When combined with existing kinematic and BSM distance estimates, we derive a mean value of $9.3 \pm 1.8$ Mpc. SN 2003gd was found to have a lower tail luminosity compared with other normal Type II-P supernovae (SNe II-P) bringing into question the nature of this SN. We present a discussion concluding that this is a normal SN II-P, which is consistent with the observed progenitor mass of $8^{+4}_{-2}$ $M_{\odot}$.

**Key words:** stars: evolution – supernovae: general – supernovae: individual: SN 2003gd – galaxies: distances and redshifts – galaxies: individual: M74.

## 1 INTRODUCTION

Supernova (SN) 2003gd was discovered by Rev. Bob Evans on 2003 June 12.82 UT (JD 245 2803.32) with an apparent magnitude of ∼13.2 mag, situated on the southern spiral arm of M74. The SN was soon confirmed by R. H. McNaught on June 13.84 UT who gave a precise position of RA $= 1^{\rm h}36^{\rm m}42\overset{\rm s}{.}65$, Dec. $= +15^{\circ}44'20\overset{''}{.}9$ (Evans & McNaught 2003). Garnavich & Bass (2003) obtained a near-infrared spectrum of the SN on June 13.46 UT showing broad Pa$\alpha$ and Pa$\gamma$, which are indicative of an SN of Type II. Kotak et al. (2003) confirmed 2003gd as a Type II with an optical spectrum and estimated that it was roughly 2 months post-explosion. Owing to the relative proximity of M74 (9.3 Mpc; see Section 4.3) and its favourable inclination, a monitoring programme was initiated. M74 was also the host galaxy of the recent Type Ic SN 2002ap (Gal-Yam, Ofek & Shemmer 2002; Mazzali et al. 2002; Smartt et al. 2002b). Van Dyk, Li & Filippenko (2003) presented early *BVRI* light curves and colour curves of SN 2003gd and compared them to those of SN 1999em. They photometrically classified 2003gd as a Type II-P supernova (SN II-P) and also gave estimates of the explosion date, 2003 March 17, and of the line-of-sight reddening, $E(B-V) = 0.13 \pm 0.03$. Using ground based astrometric calibrations, Smartt et al. (2003b) and Van Dyk et al. (2003) estimated the position of SN 2003gd on pre-discovery *Hubble Space Telescope* (*HST*) images

⋆E-mail: mah@ast.cam.ac.uk

© 2005 RAS

of M74, suggesting possible candidates for the progenitor, but both studies required follow-up *HST* images to determine the SN position with sufficient precision to unambiguously identify any precursor star.

After observing SN 2003gd with the Advanced Camera for Surveys (ACS) as part of our ongoing *HST* programme on SN progenitors, we presented the discovery of the star that exploded as SN 2003gd (Smartt et al. 2004). The progenitor star was also identified on pre-explosion Gemini images and the combined *VRI* magnitudes were used to estimate its intrinsic colour and luminosity. These were found to be consistent with those of a red supergiant (RSG) and comparison with stellar evolutionary tracks suggested that it had an initial main-sequence mass of $8^{+4}_{-2}\,M_{\odot}$. This is only the third time that a progenitor of a genuinely confirmed SN has been identified and is the first apparently normal RSG to be associated with an SN II-P. The determination of intrinsic colour and luminosity require the reddening and distance to be known. We summarized the results of our measurements for both of these quantities in Smartt et al. (2004) and here, in this paper, we present the full photometric and spectroscopic data set along with the analysis, which led to these results. Given the discovery of an RSG progenitor star, which have long been assumed to be the progenitors of SNe II-P, it is essential that the SN itself is studied and quantified.

In this paper, we present extensive photometric and spectroscopic data of SN 2003gd in Section 2, followed by an analysis of the photometry in Section 3.1, where an explosion date is estimated. We estimate the reddening towards the SN, using three different methods, in Section 3.2, and analyse the velocity evolution in Section 3.3. The distance to M74 is not well known and as yet no Cepheid distance exists. We attempt to improve the situation in Section 4 by estimating the distance using two different methods and compiling all distances within the literature. Using the distance found, we then calculate the amount of $^{56}$Ni synthesized in the explosion in Section 5. In Section 6, the observed properties of SN 2003gd are compared to the semi-analytical model of Zampieri et al. (2003) and, in Section 7, we discuss the nature of the SN and the implication for the progenitor. We then conclude in Section 8. Throughout this work, we have assumed the Galactic reddening laws of Cardelli, Clayton & Mathis (1989) with $R_V = 3.1$.

## 2 OBSERVATIONS

### 2.1 Photometry of SN 2003gd

*BVRI* photometry was obtained shortly after discovery and covers a range of ∼92–169 d after explosion with a few late-time epochs around 490 d. These data were collected from several telescopes: the 1.0-m Jacobus Kapteyn Telescope (JKT), the 2.5-m Isaac Newton Telescope (INT) and the 3.5-m Telescopio Nazionale Galileo (TNG), all on La Palma, and the 1.82-m Copernico Telescope (CTA) at Asiago, Italy. The latest data were taken with Unit Telescope 1 (UT1), Antu, of the European Southern Observatory (ESO) Very Large Telescope (VLT), Paranal, Chile. A summary of these observations can be found in Table 1, as well as the results from the optical photometry.

The JKT observations were taken with the JKT Acquisition and Guiding (JAG) unit, using the 2048 × 2048 SITe1 CCD camera and were reduced using standard techniques within IRAF. The frames were debiased and flat-fielded using twilight sky flats generally taken on the night of the observations. In some cases, flats for our required filters were not available from that night and we employed the best set of flats closest in time to the SN observations. An extensive photometric sequence of stars around M74 has been calibrated by Henden (2002), originally intended for monitoring of SN 2002ap. On the JKT images, there were normally nine stars suitable for calibration of the SN magnitudes (Henden numbers 100, 109, 149, 153, 156, 158, 160, 161) and these were used to determine the zero-points and transformation coefficients on each night. In some cases, the telescope pointing was slightly different or the brightest stars in the sequence were saturated as a result of the increased exposure time for the fading SN and hence not all the standards could be used. A minimum of three standard stars were always available on each night. The *BVRI* magnitudes were obtained using aperture photometry and the errors are the standard deviations of the individual values of the SN magnitudes determined from each calibration star.

The INT observations were taken with the Wide Field Camera (WFC) at the prime focus. The WFC consists of four thinned EEV 2k × 4k CCDs, and SN 2003gd and its calibration stars were placed on CCD4 of the mosaic. The data were reduced using the standard pipeline processing applied to all WFC images in the Cambridge archive (Irwin & Lewis 2001). Images were taken with the Harris *V* filter, and the Sloan Digital Sky Survey-like filters $r'$ and $i'$. We attempted to transform the $r'$ and $i'$ aperture magnitudes to the *RI* system of Henden using 15 stars from the Henden catalogue. We derived good fits between the instrumental magnitudes and the intrinsic $(R - I)$ and $(V - R)$ colours for the stars, and tested these on four other stars in common to the Henden and WFC catalogues. The transformations produced *VRI* magnitudes that were accurate to a mean of 0.03. However, when we transformed the SN CCD $r'i'$ magnitudes to the *RI* system, we got very unsatisfactory results. On 2003 August 25, we derived $R = 16.20$ and $I = 16.34$, which are very discrepant from our Asiago Faint Object Spectrograph and Camera (AFOSC) magnitudes taken the previous night. As the transformations for field stars proved to be reliable, the only explanation for this serious discrepancy is the strong emission line SN spectrum producing systematic differences in the colour terms compared with the stellar spectral energy distributions. Hence, we quote the *V*-band magnitude only for these two nights as the $r'i'$ transformations cannot be relied upon to produce magnitudes consistent with our previous calibrations. The errors in the magnitudes were calculated as with the JKT data.

The CTA observations were taken with the AFOSC, a focal reducer instrument, which is equipped with a Tektronix 1024 × 1024 CCD with a pixel sampling of 0.47 arcsec pixel$^{-1}$. The TNG observations were instead secured with the Device Optimized for LOw RESolution (DOLORES), which is equipped with a Loral 2k × 2k CCD with a pixel scale of 0.275 arcsec pixel$^{-1}$. The data were reduced using standard techniques within IRAF. The SN magnitudes were measured using the IRAF point spread function (PSF) fitting task DAOPHOT. This procedure allows the simultaneous fitting and subtraction of the galaxy background. For cases in which the seeing is fair, where the SN is relatively bright and its PSF well sampled, it has been found that this method produces results in excellent agreement with the template subtraction method (see Rigon et al. 2003). The errors in the derived magnitudes were calculated by combining in quadrature the standard deviation of the magnitudes found from each of the calibration stars, the PSF fitting error and the standard deviation of the magnitudes of artificial stars placed around the SN position having the SN magnitude. The photometry results, from all telescopes, are tabulated in Table 1. The earlier data are plotted in the *BVRI* light curves in Fig. 1, whereas the late-time data are shown in Fig. 11.

**Table 1.** Journal and results of optical photometry of SN 2003gd.

| Date | JD (245 0000+) | Phase (days) | *B* | *V* | *R* | *I* | Telescope + instrument | Observer |
|---|---|---|---|---|---|---|---|---|
| 2003 Jun 19 | 2809.20 | 92 | 15.47(0.02) | 14.21(0.02) | 13.68(0.02) | 13.34(0.03) | JKT+JAG | Jonker |
| 2003 Jun 20 | 2810.21 | 93 | 15.50(0.02) | 14.18(0.04) | 13.63(0.02) | 13.30(0.04) | JKT+JAG | Jonker |
| 2003 Jun 21 | 2811.21 | 94 | 15.52(0.02) | 14.24(0.04) | 13.73(0.05) | 13.33(0.03) | JKT+JAG | Jonker |
| 2003 Jun 22 | 2812.21 | 95 | 15.53(0.01) | 14.23(0.01) | 13.69(0.02) | 13.38(0.05) | JKT+JAG | Jonker |
| 2003 Jun 23 | 2813.20 | 96 | 15.57(0.02) | 14.24(0.01) | 13.71(0.01) | 13.35(0.02) | JKT+JAG | Jonker |
| 2003 Jun 27[a] | 2817.66 | 100 | 15.58(0.03) | 14.29(0.03) | 13.75(0.02) | 13.44(0.04) | TNG+DOLORES | Zampieri |
| 2003 Jun 28 | 2818.19 | 101 | 15.62(0.01) | 14.37(0.04) | 13.76(0.02) | 13.35(0.05) | JKT+JAG | Vermaas |
| 2003 Jul 02 | 2822.20 | 105 | 15.75(0.02) | 14.42(0.07) | 13.82(0.04) | – | JKT+JAG | Vermaas |
| 2003 Jul 03 | 2823.19 | 106 | 15.78(0.01) | 14.45(0.06) | 13.85(0.04) | – | JKT+JAG | Vermaas |
| 2003 Jul 08 | 2828.18 | 111 | 15.98(0.06) | 14.59(0.03) | 13.99(0.08) | 13.63(0.03) | JKT+JAG | Exter |
| 2003 Jul 11 | 2831.21 | 114 | 16.15(0.02) | 14.78(0.03) | 14.14(0.04) | 13.76(0.05) | JKT+JAG | Exter |
| 2003 Jul 12 | 2832.22 | 115 | 16.24(0.02) | 14.84(0.03) | 14.21(0.04) | 13.82(0.04) | JKT+JAG | Exter |
| 2003 Jul 14 | 2834.22 | 117 | 16.46(0.02) | 14.98(0.03) | 14.35(0.04) | 13.93(0.06) | JKT+JAG | Exter |
| 2003 Jul 15 | 2835.15 | 118 | 16.58(0.04) | 15.04(0.05) | – | – | JKT+JAG | Exter |
| 2003 Jul 16 | 2836.23 | 119 | 16.66(0.05) | 15.17(0.06) | 14.56(0.06) | 14.11(0.09) | JKT+JAG | Exter |
| 2003 Jul 19 | 2839.23 | 122 | 17.35(0.10) | 15.54(0.06) | – | – | JKT+JAG | Exter |
| 2003 Jul 21 | 2841.56 | 124 | 17.72(0.04) | 16.02(0.04) | 15.23(0.03) | 14.59(0.05) | CTA+AFOSC | Pastorello |
| 2003 Jul 23 | 2843.18 | 126 | – | 16.75(0.04) | 15.77(0.04) | – | JKT+JAG | Verley/Leon |
| 2003 Jul 24 | 2844.19 | 127 | – | 16.89(0.03) | 16.03(0.03) | – | JKT+JAG | Verley/Leon |
| 2003 Jul 26 | 2847.19 | 128 | – | 17.24(0.02) | 16.30(0.02) | – | JKT+JAG | Verley/Leon |
| 2003 Jul 27 | 2848.18 | 129 | – | 17.26(0.01) | 16.34(0.02) | – | JKT+JAG | Verley/Leon |
| 2003 Jul 28 | 2849.18 | 130 | – | 17.27(0.01) | 16.34(0.03) | – | JKT+JAG | Verley/Leon |
| 2003 Jul 29 | 2850.18 | 131 | – | 17.36(0.02) | 16.38(0.02) | – | JKT+JAG | Verley/Leon |
| 2003 Jul 30 | 2851.18 | 132 | – | 17.37(0.04) | 16.39(0.02) | – | JKT+JAG | Verley/Leon |
| 2003 Jul 31 | 2852.18 | 133 | – | 17.37(0.02) | 16.39(0.03) | – | JKT+JAG | Verley/Leon |
| 2003 Aug 07 | 2858.73 | 141 | – | 17.44(0.03) | – | 15.77(0.04) | TNG+DOLORES | Zampieri |
| 2003 Aug 08[b] | 2859.72 | 142 | 19.24(0.05) | – | 16.36(0.03) | – | TNG+DOLORES | Zampieri |
| 2003 Aug 24 | 2875.51 | 158 | 19.34(0.10) | 17.62(0.05) | 16.75(0.05) | 16.16(0.05) | CTA+AFOSC | Benetti |
| 2003 Aug 25 | 2876.71 | 159 | – | 17.56(0.05) | – | – | INT+WFC | Irwin |
| 2003 Sep 04 | 2886.61 | 169 | – | 17.64(0.05) | – | – | INT+WFC | Irwin |
| 2004 Jul 15 | 3201.69 | 485 | – | – | 20.55(0.09) | – | TNG+DOLORES | Zampieri |
| 2004 Jul 23 | 3209.65 | 493 | – | 21.33(0.26) | – | 20.30(0.24) | TNG+DOLORES | Zampieri |
| 2004 Jul 23 | 3209.91 | 493 | 21.76(0.06) | 21.32(0.07) | 20.59(0.09) | 20.31(0.04) | VLT-UT1+FORS2 | Patat/Pignata |

Notes: figures in brackets give the errors associated with the magnitudes; a full account of these errors can be found in Section 2.1.
[a] $U = 17.19$, [b] $U = 21.39$. JKT = 1.0-m Jacobus Kapteyn Telescope, La Palma. TNG = 3.5-m Telescopio Nazionale Galileo, La Palma. CTA = 1.82-m Copernico Telescope, Asiago, Italy. INT = 2.5-m Isaac Newton Telescope, La Palma. VLT-UT1 = 8.2-m ESO Very Large Telescope, Antu (UT1), Paranal, Chile.

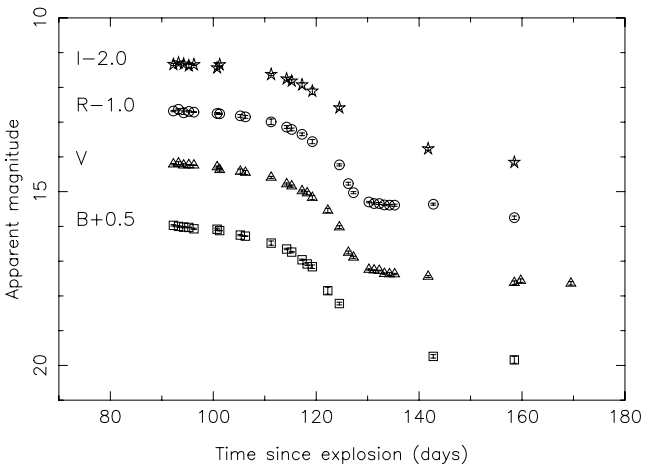


**Figure 1.** *BVRI* light curves of SN 2003gd, which have been arbitrarily shifted in magnitude for clarity.

### 2.2 Spectroscopy of SN 2003gd

Optical spectroscopic observations were taken at five telescopes and cover eight epochs, which we estimate are between 87 and 157 d after explosion, and one late-time epoch at 493 d. The log of the observations is shown in Table 2. The data were reduced using standard routines within IRAF. The frames were debiased, flat-fielded and extracted, and then wavelength calibrated using Cu–Ar and Cu–Ne lamp spectra. The wavelength calibration was checked by determining the positions of the night sky lines and small adjustments were made. The spectra were then flux calibrated using spectrophotometric flux standards observed with the same instrumental setup. The slit-widths employed were generally between 1–2.1 arcsec, hence the flux calibration is unlikely to give an accurate absolute scale. We used the *BVRI* photometry to adjust the absolute scale of the spectra at each epoch. Spectral *BVRI* magnitudes were calculated from the spectra using the IRAF package SYNPHOT within STSDAS. These magnitudes were compared with the observed photometric magnitudes and a scaling factor was calculated. The spectra were then read into the spectral analysis program DIPSO (Howarth et al. 2003) for further analysis. The earlier spectral evolution of SN 2003gd is shown in Fig. 2 and is compared to that of the well-observed SN 1999em in Fig. 3. The late-time spectrum is shown in Fig. 13 of Section 3.4. These spectra will be available through the SUSPECT[1] web site.

[1] http://bruford.nhn.ou.edu/∼suspect/

**Table 2.** Journal of spectroscopic observations of SN 2003gd.

| Date | JD (245 0000+) | Phase (days) | Range (Å) | Resolution (Å) | Instrument | Telescope | Observer |
|---|---|---|---|---|---|---|---|
| 2003 Jun 14 | 2804.72 | 87 | 3953–7499 | 4 | ISIS | WHT | Benn |
| 2003 Jun 25 | 2815.68 | 98 | 3402–9998 | 8 | IDS | INT | Lennon |
| 2003 Jun 27 | 2817.67 | 100 | 3500–10430 | ∼14 | DOLORES | TNG | Zampieri |
| 2003 Jul 09 | 2829.68 | 112 | 3200–11000 | 8 | IDS | INT | Prada |
| 2003 Jul 21 | 2841.60 | 124 | 3494–7809 | ∼24 | AFOSC | CTA | Pastorello |
| 2003 Aug 07 | 2858.71 | 141 | 3156–8066 | ∼14 | DOLORES | TNG | Zampieri |
| 2003 Aug 22 | 2873.72 | 155 | 3147–10440 | ∼14 | DOLORES | TNG | Zampieri |
| 2003 Aug 24 | 2875.55 | 157 | 3486–7475 | ∼24 | AFOSC | CTA | Benetti |
| 2004 Jul 23 | 3209.90 | 493 | 4233–9632 | ∼13 | FORS2 | VLT-UT1 | Patat/Pignata |

WHT = 4.2-m William Herschel Telescope, La Palma. TNG = 3.5-m Telescopio Nazionale Galileo, La Palma. CTA = 1.82-m Copernico Telescope, Asiago, Italy. INT = 2.5-m Isaac Newton Telescope, La Palma. VLT-UT1 = 8.2-m ESO Very Large Telescope, Antu (UT1), Paranal, Chile.

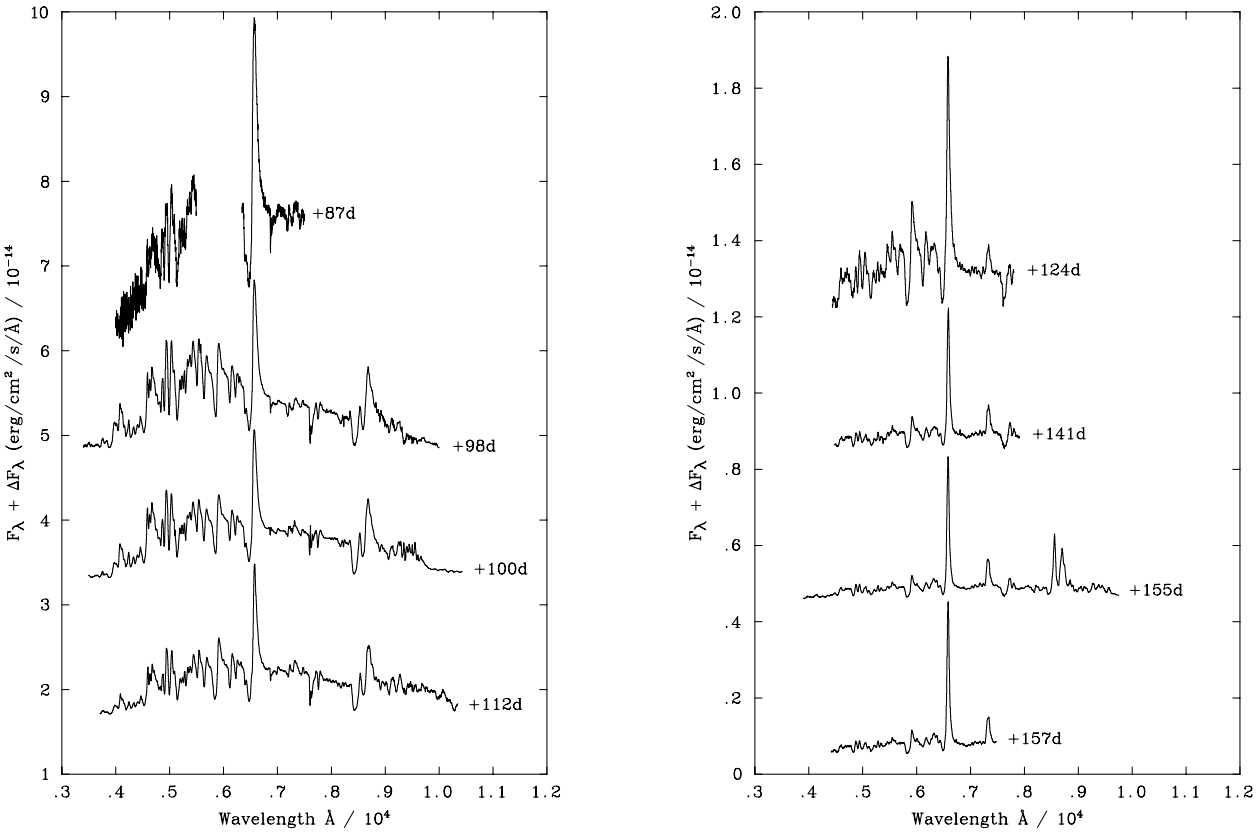


**Figure 2.** Spectral evolution of SN 2003gd from 87–157 d after explosion, where the spectra have been arbitrarily shifted in flux for clarity.

### 2.3 *HST* ACS and WFPC2 observations of M74

#### *2.3.1 ACS HRC imaging of SN 2003gd*

*BV* and *I* imaging of SN 2003gd was acquired with the High Resolution Camera (HRC) of the ACS on *HST*. SN 2003gd was observed at an epoch ∼137 d post-explosion as part of program GO9733. These observations were acquired in order to image the surroundings of the SN to determine a value of the reddening towards stars near the SN and to determine the exact location of the SN with respect to nearby stars. These observations allowed the location of the SN to be determined on pre-explosion observations and a direct identification of the progenitor star (Smartt et al. 2004). Details of the *HST* ACS observations are given in Table 3.

The on-the-fly re-calibrated (OTFR) ACS images were obtained from the Space Telescope European Coordinating Facility archive. Photometry was conducted on these frames using the IRAF package DAOPHOT (Stetson 1987) and its incorporated PSF fitting algorithm ALLSTAR (Stetson & Harris 1988). *HST* photometric system magnitudes, of stars and the SN in these images, were converted to the Johnson–Cousins system using the transformations of Holtzman et al. (1995).

#### *2.3.2 WFPC2 observations of M74*

M74 was imaged, in *B* and *I*, with the Wide Field Planetary Camera 2 (WFPC2) instrument on *HST* as part of program GO9042 although

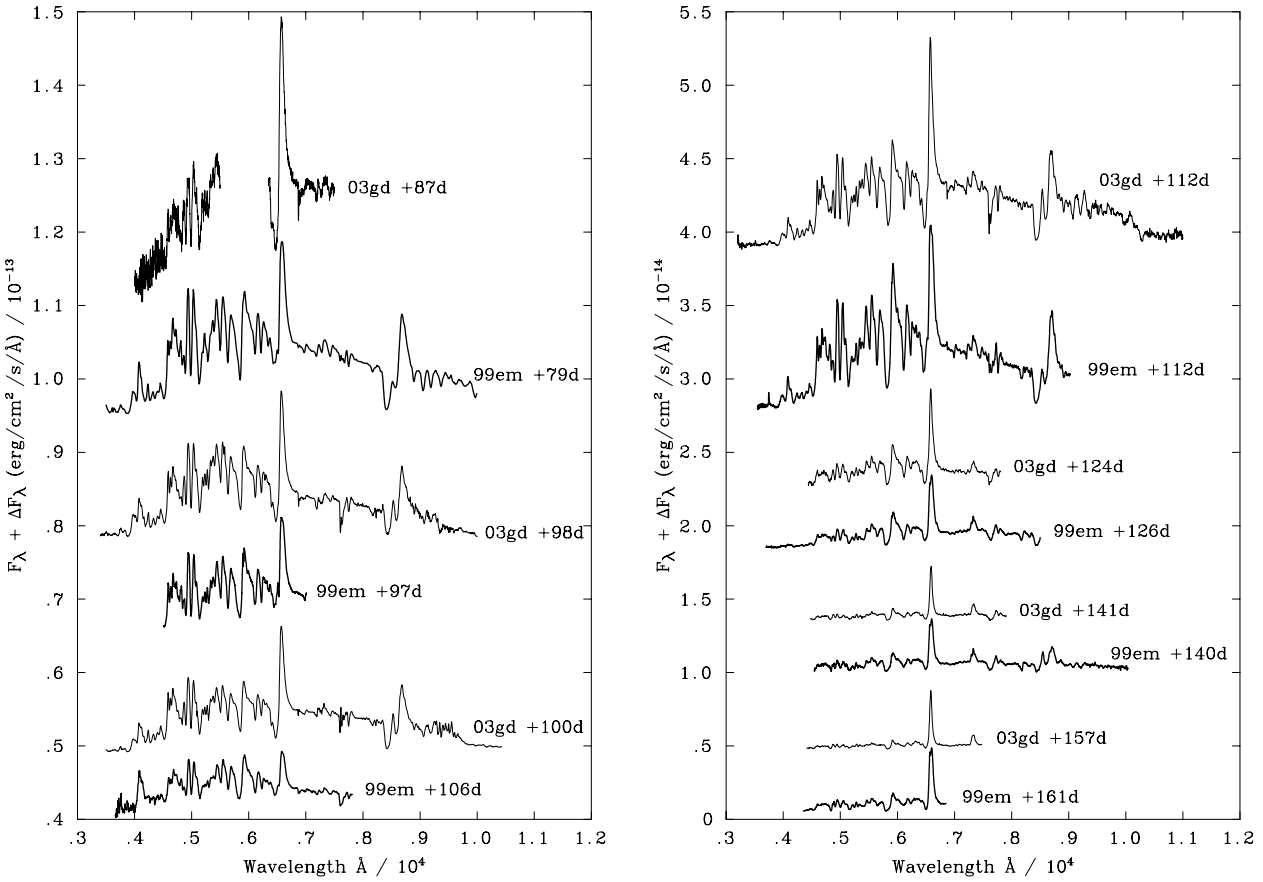


**Figure 3.** Comparison of the spectra of SN 2003gd and SN 1999em at similar phases, where the spectra have been arbitrarily shifted in flux for clarity. The spectra of both SNe show remarkable similarities at all epochs.

**Table 3.** Summary of *HST* observations of SN 2003gd and M74.

| Date | Filter | Data set | Exposure(s) | Instrument |
|---|---|---|---|---|
| 2003 Aug 1 | F439W | J8NV01011/21 | 2500 | ACS/HRC |
| 2003 Aug 2 | F555W | J8NV01031/41 | 1100 | ACS/HRC |
| 2003 Aug 2 | F814W | J8NV01051 | 1350 | ACS/HRC |
| 2001 Oct 3 | F450W | U6EA0101/02 | 460 | WFPC2 |
| 2001 Oct 3 | F814W | U6EA0103/04 | 460 | WFPC2 |

these observations did not include the location of SN 2003gd. Details of these observations are given in Table 3. The OTFR images were retrieved from the Space Telescope European Coordinating Facility archive, with cosmic ray split frames pre-combined. Photometry was conducted on these frames using the HSTPHOT version 1.15b package (Dolphin 2000a,b). HSTPHOT includes corrections for charge transfer efficiency, PSF variation and aperture size, and converts instrumental magnitudes to standard *UBVRI* magnitudes automatically. Stars, suitable for the brightest supergiants distance determination technique (see Section 4.2), were selected from the photometry output using the HSTPHOT object type classification scheme. Objects that were classified by HSTPHOT as extended, blended or containing bad pixels were discarded, as were probably blended stars or stars in crowded areas with PSF fit $\chi^2 > 2.5$.

## 3 ANALYSIS

### 3.1 Explosion epoch

The first photometric data were obtained ∼6 d after discovery. As can be seen from the *BVRI* light curves (Fig. 1), SN 2003gd was discovered close to the end of its plateau phase when the host galaxy became visible after its conjunction with the sun. The plateau phase ends ∼30 d later when the nebular tail phase begins. The light curve of SN 2003gd was compared to that of SN 1999em, a similar SN II-P, using a $\chi^2$-fitting algorithm to adjust the time and apparent magnitude to find the best fit. The SN 2003gd data from after JD 245 2845 were not included in the fit because of the difference in tail luminosities. The *BVRI* best fits are shown in Fig. 4 with the shift in time and apparent magnitude inset in each figure. The results from the $\chi^2$-fitting algorithm are shown in Table 4, as well as the weighted average of the shift in days for the *VRI* bands. Although *B* has a large reduced-$\chi^2$, the fit to the knee in the light curve looks as good as the others. The poor fit could be caused by: (i) underestimation of the errors in the photometry, or (ii) the errors being non-Gaussian as a result of the lower magnitude in the *B* band. The *B*-band data were subsequently removed from the explosion date calculation, but had they been included there would have been little difference in the result. The errors in $\Delta t$, the shift in days, and $\Delta m$, the shift in magnitude, are the errors determined from the $\chi^2$ fit at the $1\sigma$ level and are shown in brackets in Table 4. The explosion date was determined using the weighted average of

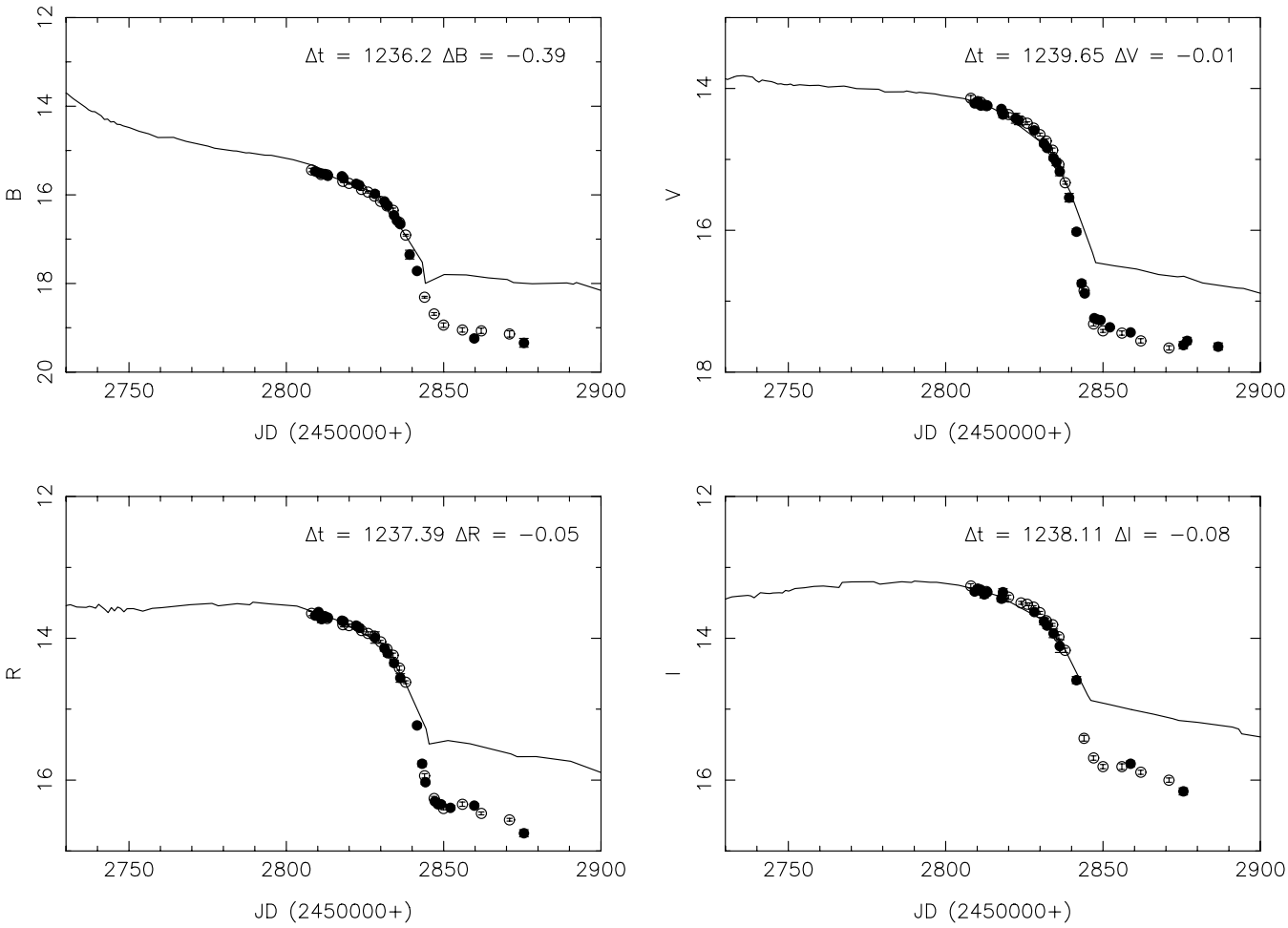


**Figure 4.** *BVRI* light curves of SN 2003gd over-plotted with the light curve for SN 1999em from Hamuy et al. (2001). Filled circles are from data in Table 1 and open circles are from Van Dyk et al. (2003) for comparison. The reduced-$\chi^2$ of the fit for *BVRI* are as follows: 6.92, 1.37, 1.02 and 0.69.

**Table 4.** Results from the $\chi^2$-fitting algorithm, which adjusts the time, $\Delta t$, and apparent magnitude, $\Delta m$, of the model light curve (SN 1999em) to find the best fit to the data points of SN 2003gd, where $\nu$ = number of data points − number of degrees of freedom.

| Filter | Reduced-$\chi^2$ | $\nu$ | $\Delta t$ (days) | $\Delta m$ |
|---|---|---|---|---|
| *B* | 6.92 | 14 | 1236.20 | −0.39 |
| *V* | 1.37 | 12 | 1239.65(0.53) | −0.01(0.02) |
| *R* | 1.02 | 12 | 1237.39(0.65) | −0.05(0.02) |
| *I* | 0.69 | 10 | 1238.11(1.14) | −0.08(0.03) |
| *VRI* | | | 1238.67(0.39) | |

$\Delta t$, in *VRI*, and the explosion epoch of SN 1999em (Hamuy et al. 2001), which was estimated as JD 245 1478.8 ± 0.5, within 2 d of Elmhamdi et al. (2003b). We find the explosion date of SN 2003gd therefore to be JD 245 2717 ± 21, which corresponds to 2003 March 18. The error in the explosion epoch was estimated from the error in the weighted average of $\Delta t$, the error in the SN 1999em explosion date and the uncertainty in the duration of the plateau of SN 2003gd. This latter uncertainty was estimated from the observed parameters of a sample of 13 SNe II-P from Hamuy (2003, table 3) where the mean plateau duration was found to be 131 ± 21 d. The most significant error is introduced by the assumption that the plateau of SN 2003gd was of a similar duration to SN 1999em. We have based this assumption on the spectral similarity of the two events (see Fig. 3 and Section 4.1) and their comparable masses (Smartt et al. 2002a; Elmhamdi et al. 2003b; Smartt et al. 2004). The error of ±21 d amply accounts for any reasonable intrinsic difference that may exist. Given this explosion epoch, we estimate that the SN was discovered ∼86 d after explosion. The light curves of both supernovae (SNe) are comparable during the plateau phase, but SN 2003gd is substantially fainter than SN 1999em in the late-time nebular phase. This is most likely the result of a lower $^{56}$Ni mass synthesized in the explosion, which was also suggested by Van Dyk et al. (2003).

### 3.2 Reddening estimation towards SN 2003gd

The reddening was estimated towards SN 2003gd using three different methods. First, it was estimated using the colours of the SN compared to SN 1999em; secondly, using *HST* photometry of the surrounding stars; and, finally, from the reddening towards nearby H II regions.

#### *3.2.1 Comparison of the colour evolution of SN 2003gd*

This method assumes that SNe II-P all reach the same intrinsic colour towards the end of the plateau phase. This is, in turn, based on the assumption that the opacity of SNe II-P is dominated by electron scattering and, therefore, the SNe should reach the temperature of hydrogen recombination at this point (Eastman, Schmidt &

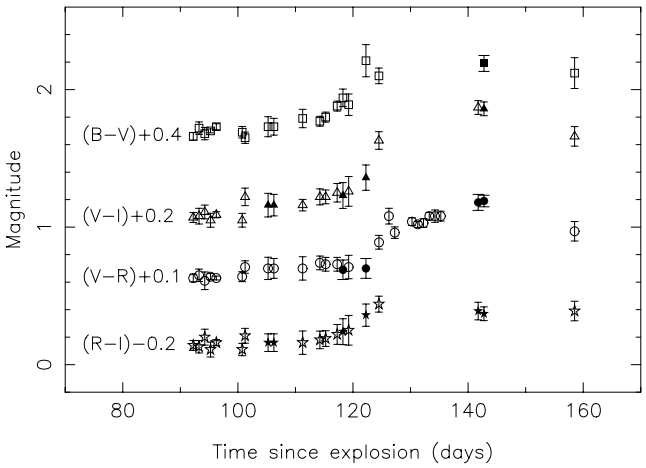


**Figure 5.** Observed $(B-V)$, $(V-R)$, $(V-I)$ and $(R-I)$ colour curves of SN 2003gd plotted against the time since explosion. Open symbols show direct observed colours, whereas filled symbols are colours determined from the interpolated light curve.

**Table 5.** Results from the $\chi^2$-fitting algorithm to determine the reddening of SN 2003gd, where $\nu$ = number of data points − number of degrees of freedom.

| Colour | Reduced-$\chi^2$ | $\nu$ | Colour excess | $A_V$ | $E(B-V)$ |
|---|---|---|---|---|---|
| $B-V$ | 2.20 | 9 | −0.16 | −0.49 | −0.16 |
| $V-R$ | 0.27 | 9 | 0.01 | 0.06 | 0.02 |
| $V-I$ | 1.01 | 7 | 0.13(0.02) | 0.31(0.05) | 0.10(0.02) |

Kirshner 1996; Hamuy 2004a). As shown in Section 2.2, the two SNe are strikingly similar at all epochs of our sample. It is therefore reasonable to assume that SN 2003gd would indeed reach the same colour as SN 1999em. Hamuy (2004a) investigated this method using a sample of 24 SNe II-P with *BVI* photometry using SN 1999em as the comparison SN. Hamuy (2004a) found serious discrepancies between the results obtained from $(B-V)$ and $(V-I)$ colours, and noted that this is an unsatisfactory technique and other methods should be explored in future.

Bearing this in mind, we carried out the analysis using $(B-V)$, $(V-R)$ and $(V-I)$. These colour curves for SN 2003gd can be seen in Fig. 5. SN 1999em was extensively modelled by Baron et al. (2000), who determined a hard upper limit of $E(B-V) \leqslant 0.15$ and estimated a likely reddening of $E(B-V) \simeq 0.05$–$0.10$. In this paper, we adopt a reddening of $E(B-V) = 0.075 \pm 0.025$ for SN 1999em. The colour curves of SN 1999em were first dereddened using this value and were then shifted in time using the weighted average of $\Delta t$ discussed in Section 3.1. A $\chi^2$-fitting algorithm was then used to compare the colours of SN 2003gd with those of SN 1999em for JD < 245 2830, the end of the plateau phase. The results of the $\chi^2$ fit are listed in Table 5 and shown in Fig. 6. The errors in the colour excess, shown in brackets, were estimated from the $\chi^2$ fit at the $1\sigma$ level. The systematic error, that the uncertainty in the reddening of SN 1999em introduces, was excluded from the fit to be added later.

Hamuy (2004a) finds the $(V-I)$ reddening estimate to be better behaved than the $(B-V)$ estimate and, in the case of SN 2003gd, we find this also to be true. The $(B-V)$ fit yields a negative reddening that is unphysical and could be the result of line blanketing as suggested by Hamuy. The $(V-R)$ estimate also gives an unrealistically small reddening value, which is less than the Galactic reddening of

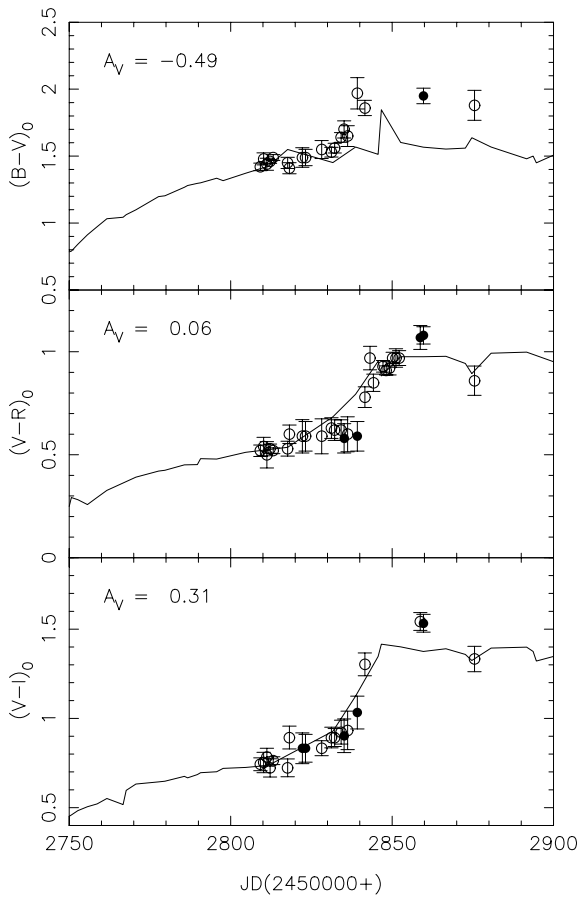


**Figure 6.** $(B-V)$, $(V-R)$ and $(V-I)$ colour evolutions of SN 2003gd compared with the intrinsic colour evolutions of SN 1999em (Hamuy et al. 2001). The visual extinction required for each fit is given in the panels. The reduced-$\chi^2$ for $(B-V)$, $(V-R)$ and $(V-I)$ are 2.20, 0.27 and 1.01, respectively. Open circles show direct observed colours whereas filled circles are colours determined from the interpolated light curve.

$E(B-V) = 0.07$ (Schlegel, Finkbeiner & Davis 1998). In any case, the reduced-$\chi^2$ values for the $(B-V)$ and $(V-R)$ are indicative of poor fits and were excluded from the reddening estimate. Using the $(V-I)$ colour fit, we estimate the reddening to be $E(B-V) = 0.10 \pm 0.03$, which is comparable to that determined by Van Dyk et al. (2003). The error was determined by combining in quadrature the error from the $\chi^2$ fit and the systematic error in the reddening of SN 1999em. The error that the uncertainty in the explosion date introduces was found to be negligible.

### *3.2.2 Reddening towards the neighbouring stars*

Three-colour ACS photometry (see Section 2.3.1) was used to estimate the reddening towards SN 2003gd. $(B-V)$ and $(V-I)$ colours of 25 stars within 6 arcsec of SN 2003gd were compared with the intrinsic supergiant colour sequence of Drilling & Landolt (2000). The reddening was calculated using a $\chi^2$ minimization of the displacement of the stars from the intrinsic supergiant colour sequence, for a range of values of $E(B-V)$. The reddening vector, in the $(B-V)/(V-I)$ colour plane, assumed the reddening laws of Cardelli et al. (1989) with $R_V = 3.1$. Using this method the reddening was estimated as $E(B-V) = 0.13 \pm 0.07$. The positions of the 25 dereddened stars and the intrinsic supergiant colour sequence, on the $(B-V)/(V-I)$ colour plane, are shown in Fig. 7.

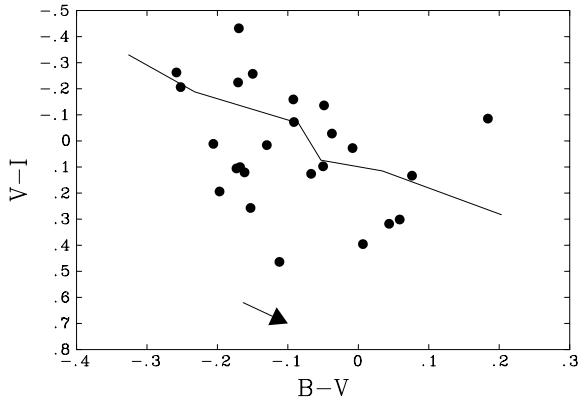


**Figure 7.** A two colour diagram showing 25 stars, of M74, within 6 arcsec of the location of SN 2003gd. The stars have been dereddened by $E(B-V) = 0.13$. The intrinsic colour sequence of supergiants (Drilling & Landolt 2000) is shown with the solid line. The reddening vector is indicated by the arrow.

**Table 6.** Nearby H II regions to SN 2003gd in M74 analysed by Belley & Roy (1992).

| H II region | $c(\mathrm{H}\beta)$ | $A_V$ | $E(B-V)$ |
|---|---|---|---|
| 72 | 0.47 | 1.01 | 0.33 |
| 73 | 0.06 | 0.13 | 0.04 |
| Mean | | | 0.19(0.15) |

**Table 7.** Summary of the results from the three methods used in determining the reddening of SN 2003gd.

| Method | $E(B-V)$ |
|---|---|
| Comparison with SN 1999em | 0.10(0.03) |
| *HST* photometry | 0.13(0.07) |
| Nearby H II regions | 0.19(0.15) |
| Mean | 0.14(0.06) |

### *3.2.3 Reddening towards nearby H II regions*

The abundance gradient in M74 has been studied by Belley & Roy (1992), who observed the nebular lines of 132 H II regions. For each H II region, the authors calculated an extinction at H$\beta$, which gives the total extinction, i.e. a combined Galactic plus extragalactic extinction. The closest H II regions to SN 2003gd, which were analysed, are Belley & Roy numbers 72 and 73. The logarithmic extinction $c(\mathrm{H}\beta)$, visual extinction $A_V$ and the colour excess $E(B-V)$ for these H II regions are given in Table 6 along with their mean. The visual extinction was calculated from the logarithmic extinction and an extinction relationship of $A_{4861}/A_V = 1.16$ with $R_V = 3.1$ (Cardelli et al. 1989).

### *3.2.4 Visual extinction of SN 2003gd*

A summary of the results of the methods discussed is given in Table 7 along with the mean of the methods, $E(B-V) = 0.14 \pm 0.06$. The error on the mean was found to be unrealistically small at 0.03, therefore we have quoted the combined errors of the three methods.

**Table 8.** Velocities derived from the minimum of the Fe II $\lambda$5169 line for SN 2003gd.

| Date | JD (245 0000+) | Phase (days) | $v_{\mathrm{Fe\,II}\lambda5169}$ (km s$^{-1}$) |
|---|---|---|---|
| 2003 Jun 14 | 2804.72 | 87 | 2514(237) |
| 2003 Jun 25 | 2815.68 | 98 | 2282(126) |
| 2003 Jun 27 | 2817.67 | 100 | 2398(126) |
| 2003 Jul 09 | 2829.68 | 112 | 2050(126) |
| 2003 Jul 21 | 2841.60 | 124 | 1934(126) |
| 2003 Aug 07 | 2858.71 | 141 | 1876(872) |
| 2003 Aug 22 | 2873.72 | 155 | 1586(525) |
| 2003 Aug 24 | 2875.55 | 157 | 1237(126) |

**Table 9.** Velocities derived from the minimum of the Fe II $\lambda$5169 line for SN 1999em using the technique described here.

| Date | JD (245 0000+) | Phase (days) | $v_{\mathrm{Fe\,II}\lambda5169}$ (km s$^{-1}$) | Spectral source |
|---|---|---|---|---|
| 1999 Nov 09 | 1492.14 | 13 | 7101(271) | 1 |
| 1999 Nov 14 | 1496.67 | 18 | 6088(182) | 2 |
| 1999 Nov 19 | 1501.66 | 23 | 5268(173) | 2 |
| 1999 Dec 15 | 1527.74 | 49 | 3722(378) | 1 |
| 1999 Dec 17 | 1529.74 | 51 | 3542(294) | 1 |
| 1999 Dec 18 | 1530.70 | 52 | 3394(311) | 3 |
| 1999 Dec 29 | 1541.70 | 63 | 3250(287) | 3 |
| 1999 Dec 31 | 1543.66 | 66 | 3098(272) | 2 |
| 2000 Jan 13 | 1556.84 | 78 | 2834(189) | 1 |
| 2000 Feb 01 | 1575.74 | 97 | 2439(360) | 1 |
| 2000 Feb 09 | 1584.35 | 106 | 2173(263) | 3 |
| 2000 Feb 16 | 1590.55 | 112 | 2207(341) | 3 |
| 2000 Mar 01 | 1604.74 | 126 | 1855(569) | 1 |
| 2000 Mar 13 | 1616.51 | 138 | 1477(353) | 3 |
| 2000 Mar 15 | 1618.64 | 140 | 1306(305) | 1 |

(1) Leonard et al. (2002a), (2) Hamuy et al. (2001), (3) Elmhamdi et al. (2003b).

The Galactic extinction law with $R_V = 3.1$ was used to calculate the visual extinction, which was found to be $A_V = 0.43 \pm 0.19$.

## 3.3 Expansion velocity of SN 2003gd

We measured the expansion velocity of the ejecta of SN 2003gd from the minimum of the blueshifted absorption trough of the Fe II $\lambda$5169 line, as in Hamuy (2004b). This absorption line is asymmetric and shows signs of blending, possibly with Ti II and Mg I $\lambda$5167 (Pastorello 2003). The absorption trough was fitted by three Gaussians using the Emission Line Fitting (ELF) package within the Starlink spectral analysis package DIPSO. The minimum was found from the convolution of the three Gaussians and the error was estimated from the difference between this and a single Gaussian fit. The velocities measured in this way for SN 2003gd are listed in Table 8. As a consistency check, several epochs of SN 1999em, from Hamuy et al. (2001), Leonard et al. (2002a) and Elmhamdi et al. (2003b), were also measured using the same technique. The velocities measured here are listed in Table 9. The velocity evolutions of SNe 2003gd and 1999em are plotted in Fig. 8.

The velocity evolution of SN 2003gd closely follows that of SN 1999em at all epochs. As the SNe age, it becomes increasingly difficult to measure the minimum of the Fe II $\lambda$5169 line as a blended

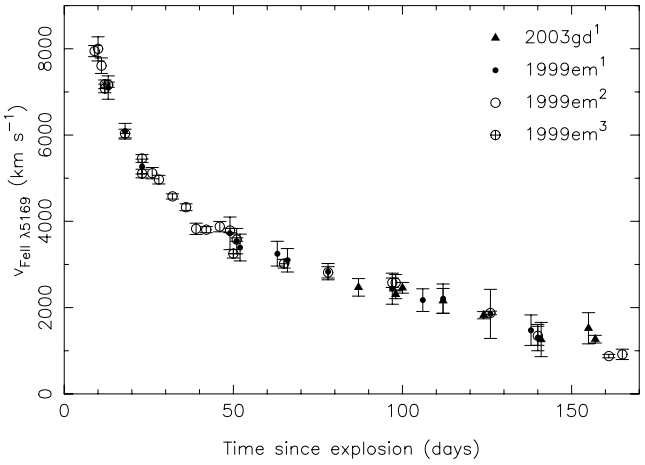


**Figure 8.** Velocity evolution of SN 2003gd and SN 1999em derived from the minimum of the blueshifted absorption trough of Fe II λ5169. The superscripts in the figure denote the source of the velocity measurements: (1) this paper, (2) Leonard et al. (2002a), (3) Hamuy et al. (2001).

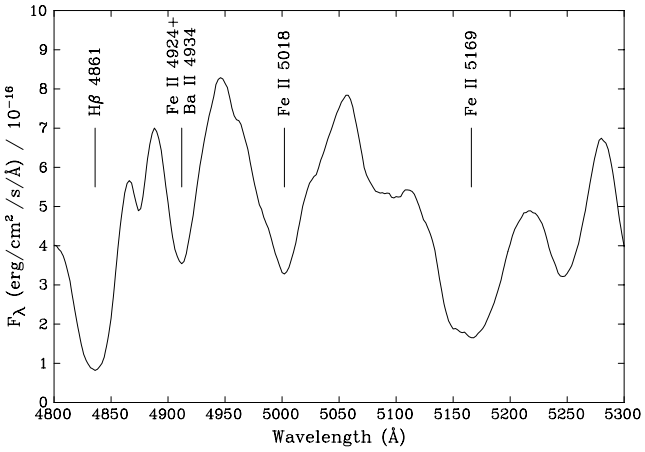


**Figure 9.** Spectrum of SN 1999em (Leonard et al. 2002a) from 161 d after explosion showing blend appearing in the Fe II λ5169 line.

trough begins appearing as shown in Fig. 9. The velocity measurements carried out in this work on the spectra of Hamuy et al. (2001), Leonard et al. (2002a) and Elmhamdi et al. (2003b) are comparable with the existing measurements. This demonstrates the consistency of the techniques used. Although the methods are consistent, we propose that the Fe II λ5169 line is not a good indication of the ejecta velocity at later epochs. Fig. 10 shows the velocities derived from the Fe II λλ4924, 5018, 5169 lines, taken from Leonard et al. (2002a), which are traditionally used to determine the photospheric velocity. These authors, however, point out the consistently lower velocity derived from the Fe II λ4924 line compared with those calculated from the other Fe II lines. Leonard et al. suggest that this is caused by significant blending with Ba II λ4934, which was also found by Pastorello (2003). Fig. 10 demonstrates this, but also shows that the Fe II λ5169 line, at around 140 d, gives significantly lower velocities. Although Fe II λ5169 yields lower velocities at these epochs, for our purposes of comparison, this is of little consequence.

### 3.4 Late-time photometry and spectroscopy

Late-time photometry was obtained around 490 d after explosion and is plotted in Fig. 11 along with the nebular phase photometry.

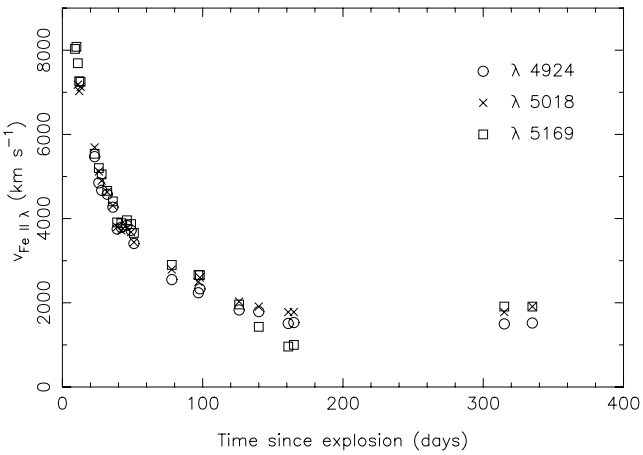


**Figure 10.** Velocity evolution of SN 1999em derived from the minimum of the blueshifted absorption troughs of FeII λλ4924, 5018, 5169, taken from Leonard et al. (2002a).

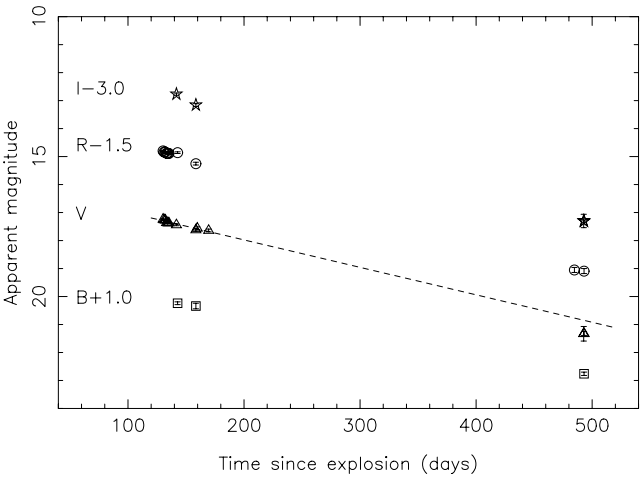


**Figure 11.** *BVRI* nebular and late-time photometry of SN 2003gd with a linear fit of the earlier nebular data, in the *V* band, shown with a dashed line. The late-time photometry, in the *V* band, is lower than what we would expect from the earlier photometry.

The details of these observations can be found in Table 1. A linear fit, which is shown with the dashed line, has been applied to the early nebular phase data in the *V* band. The decay rate from this fit was estimated to be 0.98 mag 100 d$^{-1}$, which corresponds to the decay rate of $^{56}$Co, suggesting that little or no $\gamma$-rays escaped during this time. The pseudo-bolometric (hereafter denoted by UVOIR, see Section 7.1) light curve is shown in Fig. 12 where the dashed line is the fit to the early nebular data and the dotted line is the decay slope of $^{56}\mathrm{Co} \rightarrow {}^{56}\mathrm{Fe}$. A late-time spectrum was also obtained, around 493 d after explosion, and is shown in Fig. 13 alongside the penultimate spectrum of SN 2003gd and a spectrum of SN 1999em of a similar epoch.

Fig. 11 shows a deficit in the latest value of the *V*-band luminosity when compared with that expected from the linear fit. This deficit could either be the result of dust formation or the SN becoming more transparent to $\gamma$-rays, allowing leakage to occur, or a combination of both. The fit in Fig. 12, which is shown by the dashed line, would suggest that the latest point is actually brighter than expected, but it is difficult to draw any conclusions because of the limited data in the tail. If we assume the $\gamma$-rays are fully thermalized, as the fit to

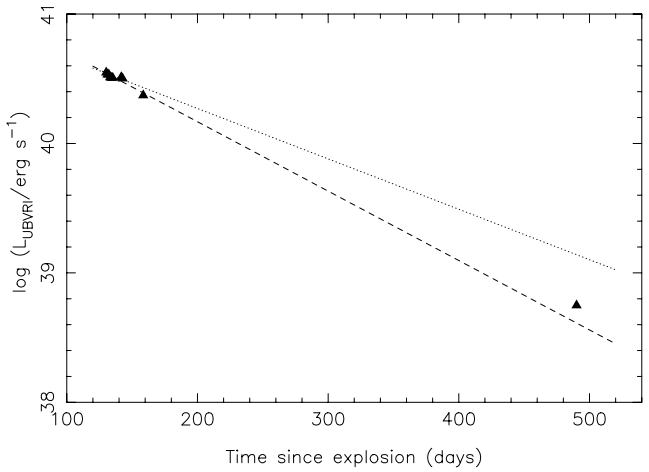


**Figure 12.** Pseudo-bolometric (UVOIR) light curve of SN 2003gd with a linear fit of the earlier nebular data shown with a dashed line and the decay slope of $^{56}$Co $\rightarrow$ $^{56}$Fe shown with a dotted line.

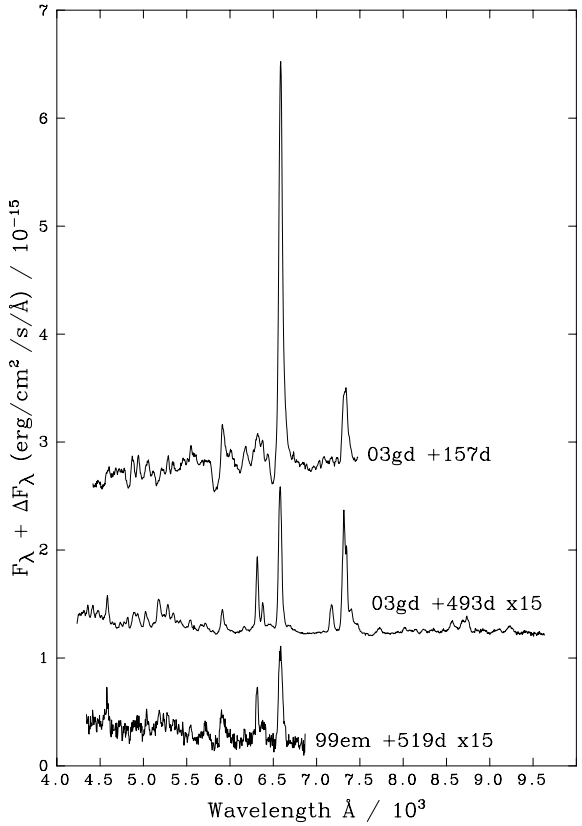


**Figure 13.** Late-time spectrum of SN 2003gd at 493 d shown with its penultimate spectrum and a spectrum of SN 1999em of a similar epoch.

the *V*-band data would suggest, then the luminosity is substantially less than what we would expect. Elmhamdi et al. (2003b) noted a blueshift of the line profiles of [O I] λλ6300, 6364 Å and Hα, and attributed this to the formation of dust. Fig. 14 shows the profiles of Hα from three epochs: 124, 157 and 493 d post-explosion, where the vertical line marks the maximum of the Hα emission from the earliest spectrum. The peak of the Hα emission from 157 d shows a slight redshift, but the latest spectrum clearly shows a skewing towards the blue. The [O I] λλ6300, 6364 Å lines, however, are not clear enough

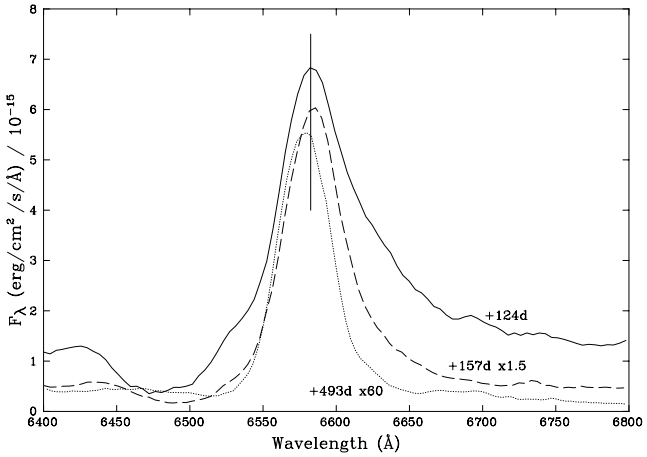


**Figure 14.** Hα profiles of SN 2003gd from 124, 157 and 493 d post-explosion. The vertical line marks the maximum of the Hα emission from the earliest spectrum. The peak of the Hα emission from 157 d shows a slight redshift of the peak, but the latest spectrum clearly shows a shift to the blue.

in the earlier spectra to verify this blueshift. Nevertheless, the drop in luminosity at late-times, combined with the apparent blueshift of the Hα emission, does indeed suggest dust formed between 157 and 490 d.

## 4 DISTANCE ESTIMATES TO M74

### 4.1 Type II-P standard candle method distance estimate

Kowal (1968) first suggested that Type Ia SNe (SNe Ia) could be useful distance indicators as their peak magnitudes and redshifts were found to be closely correlated. From observations of high-*z* SNe, it is possible to measure the history of the expansion of the universe. In recent years many separate studies have been carried out using this SNe Ia method. One of the most recent studies, carried out by Tonry et al. (2003), confirmed the results of two previous studies, by Perlmutter et al. (1999) and Riess et al. (1999), who found that the universe is actually accelerating. There is currently great debate on whether SNe Ia are in fact standard candles and work on methods of standardizing these SNe is underway (Altavilla et al. 2004, and references therein). In order to verify the results from SNe Ia methods, Hamuy & Pinto (2002) investigated the plateau subclass of Type II SNe (SNe II-P) for use as standard candles. Although SNe II-P showed a wide range of luminosities at all epochs, Hamuy & Pinto (2002) showed that the velocity of the ejecta of SNe II-P and their bolometric luminosities during the plateau phase are highly correlated. Hamuy & Pinto (2002) formulated a standard candle method (SCM) for SNe II-P, which can be solved for the Hubble constant, provided a suitable distance calibrator is known. Hamuy in two further papers (Hamuy 2004a,b) first confirmed the SCM using a sample of 24 SNe II-P and then calibrated the Hubble diagram with known Cepheid distances to four of these SNe. Hamuy (2004b) calculated the Hubble constant, using $V$ and $I$ data, to be $H_0(V) = 75 \pm 7$ km s$^{-1}$ Mpc$^{-1}$ and $H_0(I) = 65 \pm 12$ km s$^{-1}$ Mpc$^{-1}$. In this paper, we use the weighted average of these results, $H_0 = 72 \pm 6$ km s$^{-1}$ Mpc$^{-1}$, which is comparable to $H_0 = 71 \pm 2$ km s$^{-1}$ Mpc$^{-1}$ derived as part of the *HST* Key Project using SNe Ia (Freedman et al. 2001). This result demonstrates the integrity of this method.

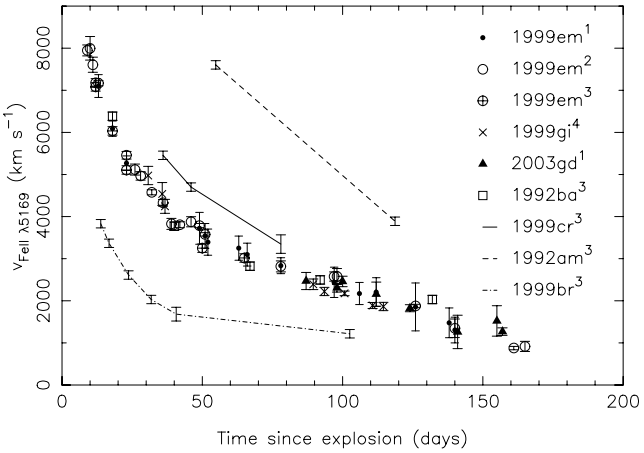


**Figure 15.** Velocity evolution of SN 2003gd compared with other similar SNe II-P (1999em, 1999gi and 1992ba) and contrasting SNe II-P (1999cr, 1992am and 1999br). The superscripts in the figure denote the source of the velocity measurements: (1) this paper, (2) Leonard et al. (2002a), (3) Hamuy et al. (2001) and (4) Leonard et al. (2002b).

We use the results from Hamuy (2004b) conversely to estimate the distance to SN 2003gd, using equations (1) and (2):

$$D(V) = \frac{10^{(1/5)[V_{50}-A_V+6.249(\pm1.35)\log(v_{50}/5000)+1.464(\pm0.15)]}}{H_0}, \quad (1)$$

$$D(I) = \frac{10^{(1/5)[I_{50}-A_I+5.445(\pm0.91)\log(v_{50}/5000)+1.923(\pm0.11)]}}{H_0}, \quad (2)$$

where $V_{50}$, $I_{50}$ and $v_{50}$ are the $V$ and $I$ magnitudes, and the expansion velocity, in km s$^{-1}$, at day 50. As SN 2003gd was in conjunction with the sun 50 d after explosion, we need to infer these quantities.

The velocity evolution of SN 2003gd and SN 1999em is shown in Fig. 8. In order to infer the velocity of SN 2003gd at day 50 from SN 1999em, it is necessary to determine whether the evolution of SN 1999em is common to other similar SNe II-P or if it is in any way peculiar. Fig. 15 shows the expansion velocities of SN 2003gd compared to other similar SNe II-P (SNe 1999em, 1999gi and 1992ba) and contrasting SNe II-P (1999cr, 1992am and 1999br). In all cases, apart from SN 1999gi, the ejecta velocities were measured from the minimum of the blueshifted absorption trough of the Fe II λ5169 line. In the case of SN 1999gi, the velocities were measured from the minimum of the available weak, unblended line features (Leonard et al. 2002b). SNe 1999em, 1999gi, 1992ba are all very similar SNe II-P with comparable velocities at day 50, $v_{50}$, and towards the end of the plateau phase. The close correspondence of the velocities of these SNe with 2003gd later in the plateau phase (∼100 d) suggests that SN 2003gd would also have had a similar $v_{50}$. To illustrate the difference between these and other SNe II-P, with quite contrasting velocity evolutions, we plot SNe 1999cr, 1992am and 1999br. Within the sample of SNe II-P studied, there is no known example of an SN II-P that has a velocity evolution similar to that of SN 2003gd between 80–130 d which then diverges from the 1999em/1999gi/1992ba slope at day 50. This assumption allows us to estimate the velocity of SN 2003gd at day 50. Because of the similarities between SN 2003gd and SN 1999em, we take the weighted average of three independent measurements of $v_{50}$ for SN 1999em and adopt this for SN 2003gd. The independent measurements are from Hamuy et al. (2001), Leonard et al. (2002a) and this paper, giving an adopted value of $v_{50} = 3694 \pm 981$ km s$^{-1}$ for SN 2003gd, where the error is the standard deviation of $v_{50}$ in the sample of 22 SNe II-P from Hamuy (2004b). The two extreme SNe, 1992am and 1999br, were excluded in this standard deviation calculation because of their peculiarities.

The apparent magnitudes for SN 2003gd at day 50 were estimated using $\Delta m$ from the $\chi^2$-fitting results (Table 4), and $V_{50}$ and $I_{50}$ magnitudes for SN 1999em (Hamuy 2004b), giving $V_{50} = 13.97 \pm 0.50$ and $I_{50} = 13.27 \pm 0.52$ for SN 2003gd. The errors adopted are the following errors combined in quadrature.

(i) The error in the magnitude at day 50 for SN 1999em.
(ii) The error in the $\chi^2$ fit.
(iii) An error associated with the assumption that the light curves of SNe 2003gd and 1999em are intrinsically the same. We have estimated this from the standard deviation in the absolute magnitudes of SNe 1992ba, 1999em and 1999gi (Hamuy 2003), giving $\langle M_V \rangle = -15.92 \pm 0.49$, $\langle M_I \rangle = -16.35 \pm 0.49$.
(iv) An error associated with the plateau length, which was taken to be 0.09 mag in $V$ and 0.17 mag in $I$.

We use the reddening estimated in Section 3.2 to give $A_V = 0.43 \pm 0.19$ and $A_I = 0.26 \pm 0.11$. Using the SCM equations (equations 1 and 2) and the inferred values of $v_{50}$, $V_{50}$ and $I_{50}$ for SN 2003gd discussed, we determine the distance in each band to be $D(V) = 9.52 \pm 4.14$ Mpc and $D(I) = 9.67 \pm 3.82$ Mpc. A weighted average yields a value of $D = 9.6 \pm 2.8$ Mpc. This error is statistical and comes from combining the uncertainties of each parameter in the SCM equations. Hamuy (2004b) finds a dispersion in the Hubble diagram of 0.3 mag, which translates to a precision of 15 per cent for extragalactic distances. The distance estimate of M74 has a greater uncertainty, as we have adopted large errors to adequately cover the assumptions we have made.

We could also estimate the distance of SN 2003gd by using the Cepheid distance to SN 1999em (Leonard et al. 2003, 11.71 ± 0.99 Mpc) directly. If we assume both SNe have the same absolute magnitudes, we can use the distance modulus for NGC 1637 and apply a correction for the difference in apparent magnitudes, shown in equation (3), to calculate the distance modulus of SN 2003gd. We use the results given in Table 4 and the visual extinction of Section 3.2:

$$\begin{aligned}\mu^{03gd} &= m_0^{03gd} - M^{03gd} \\ &= m^{03gd} - A_\lambda^{03gd} - M^{03gd} \\ &= m^{99em} + \Delta m - A_\lambda^{03gd} - M^{03gd} \\ &= m_0^{99em} + A_\lambda^{99em} + \Delta m - A_\lambda^{03gd} - M^{99em} \\ &= \mu^{99em} + \Delta m + A_\lambda^{99em} - A_\lambda^{03gd}. \end{aligned} \quad (3)$$

Using this equation and the $VRI$ data, we calculate $\mu(V) = 30.05 \pm 0.57$, $\mu(R) = 30.15 \pm 0.56$ and $\mu(I) = 30.16 \pm 0.54$. Together these give a weighted average of $\mu = 30.12 \pm 0.32$ or $D = 10.6 \pm 1.6$ Mpc, which is in agreement with our SCM distance estimate.

### 4.2 Brightest supergiants distance estimate using *HST* photometry

This method uses the correlation between the average luminosity of the brightest supergiants and the host galaxy luminosity to estimate the distance. This average luminosity should be independent of the host galaxy luminosity for there to be no distance degeneracy. This method has previously been used by Sharina, Karachentsev & Tikhonov (1996) and Sohn & Davidge (1996) to estimate the distance to M74, yielding similar results. Sohn & Davidge (1996) used

**Table 10.** Luminosity functions of blue and red supergiants in the $B$ band, where $n_{\rm BSG}$ and $n_{\rm RSG}$ are the number of blue and red supergiants, respectively, and $n_{\rm fg}$ is the number of foreground stars predicted from Bahcall & Soneira (1981), field 11.

| $B$ | $n_{\rm BSG}$ | $n_{\rm RSG}$ | $n_{\rm fg}$ |
|---|---|---|---|
| 17–18 | 1(1) | 0(0) | 0.3 |
| 18–19 | 0(0) | 1(1) | 0.5 |
| 19–20 | 0(0) | 0(0) | 0.6 |
| 20–21 | 6(2) | 3(2) | 0.8 |
| 21–22 | 71(8) | 10(3) | 0.9 |
| 22–23 | 336(18) | 37(6) | 1.1 |
| 23–24 | 1007(32) | 181(13) | 1.3 |
| 24–25 | 484(22) | 217(15) | 1.5 |
| 25–26 | 21(5) | 72(8) | 1.7 |

**Table 11.** Luminosity functions of blue and red supergiants in the $I$ band, where $n_{\rm BSG}$ and $n_{\rm RSG}$ are the number of blue and red supergiants, respectively, and $n_{\rm fg}$ is the number of foreground stars predicted from Bahcall & Soneira (1981), field 11.

| $I$ | $n_{\rm BSG}$ | $n_{\rm RSG}$ | $n_{\rm fg}$ |
|---|---|---|---|
| 17–18 | 1(1) | 1(1) | 1.1 |
| 18–19 | 0(0) | 3(2) | 1.4 |
| 19–20 | 4(2) | 5(2) | 1.8 |
| 20–21 | 23(5) | 21(5) | 2.2 |
| 21–22 | 138(12) | 109(10) | 2.6 |
| 22–23 | 650(26) | 287(17) | 2.8 |
| 23–24 | 1060(33) | 95(10) | 2.8 |
| 24–25 | 43(7) | 6(2) | 2.8 |
| 25–26 | 7(3) | 0(0) | 2.8 |

photometry of supergiants in the disk of M74 and found $\mu = 29.3$, whereas Sharina et al. (1996) calculated the mean modulus of the group of M74 and its dwarf companions as $\mu = 29.46$. Both of these studies used ground based imaging to determine the magnitudes and colours of the brightest stars. The resolution of these images hinders the viability of the method (as discussed in Section 4.3), hence we have repeated this method with *HST* photometry of M74.

We have used the method of Sohn & Davidge (1996) to determine the magnitude of the brightest supergiants. Their method first divides the supergiants into blue and red using their $(V - R)$ colours. The authors used $(V - R) = 0.5$, which, taking into account the foreground reddening of M74, corresponds approximately to an F8 supergiant (Drilling & Landolt 2000, table 15.7). The luminosity functions of blue and red supergiants then tell us the luminosity of the brightest supergiants, whilst removing contamination from foreground stars. This is accomplished by choosing the bin with statistically more supergiants than foreground stars and adopting this magnitude for the brightest supergiants. The number of foreground stars were calculated from field 11 of Bahcall & Soneira (1981). In this work, we have used an excess, of supergiants-to-foreground stars, of $2\sigma$ to indicate a significant detection.

The *HST* (WFPC2, see Section 2.3.2) photometry was first dereddened using the foreground extinction towards M74 from Schlegel et al. (1998) using the NED interface.[2] The supergiants were divided into blue and red using their $(B - I)$ colours and the intrinsic colour

[2] http://nedwww.ipac.caltech.edu/forms/calculator.html

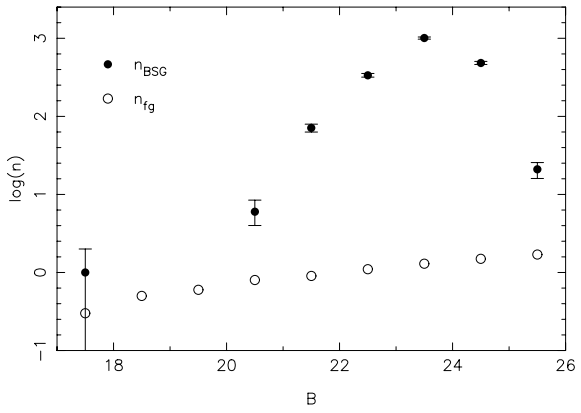


**Figure 16.** Luminosity function in the $B$ band for blue supergiants (BSGs) where $(B - I) < 1.28$ in M74.

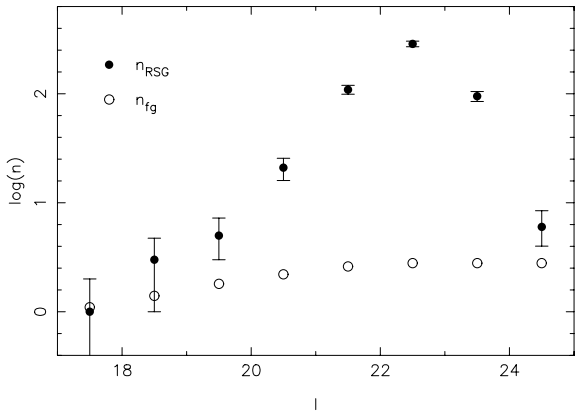


**Figure 17.** Luminosity function in the $I$ band for red supergiants (RSGs) where $(B - I) \geqslant 1.28$ in M74.

of Drilling & Landolt (2000, table 15.7) for F8-type supergiants, i.e. $(B - I) = 1.28$. We have assumed that supergiants with $(B - I) < 1.28$ are blue supergiants (BSGs) and supergiants with $B - I \geqslant 1.28$ are red supergiants (RSGs). The supergiants were then divided into luminosity bins and counted, where $n_{\rm BSG}$ and $n_{\rm RSG}$ are the number of blue and red supergiants within the bin, respectively. The resulting luminosity functions for blue and red supergiants are listed in Tables 10 and 11, and are plotted in Figs 16 and 17, in $B$ and $I$, respectively.

The number of foreground stars were calculated from the predictions of Bahcall & Soneira (1981) and scaled to the WFPC2 field-of-view of 5.0 arcmin$^2$. A significant statistical excess of BSGs was found in the range $B = 20$–$21$ and RSGs in the range $I = 20$–$21$. The $B$ magnitude of the brightest BSGs was taken to be in the middle of this bin, $B = 20.5 \pm 0.5$. Using the calibrations of Rozanski & Rowan-Robinson (1994, figs 10c, f) for BSGs and the apparent $B$ magnitude of M74 (Shostak & van der Kruit 1984, $B = 9.77$), the distance moduli were calculated. Because their calibrations for RSGs are only for the $K$ and $V$ bands, we converted our $I$ magnitudes to $V$ magnitudes. Rozanski & Rowan-Robinson warn against this and point out that the brightest stars in one band will not necessarily be the brightest in another. We therefore chose the three bluest stars in the $I = 20$–$21$ bin. We averaged their $B - I$ colours and their $I$ magnitudes and used the intrinsic colours of Drilling & Landolt (2000, table 15.7) to convert them to a $V$-band magnitude. We obtain $I = 20.6$ with $B - I = 1.3$, which corresponds to a F8-G0 supergiant with a $(V - I)$ colour of 0.7 and magnitude of $V = 21.4$. We

**Table 12.** Results of the brightest supergiants distance estimate.

| | 10(a) | 10(c) | 10(d) | 10(f) |
|---|---|---|---|---|
| M74 | 29.70(0.92) | 29.47(1.03) | 29.40(0.90) | 29.15(1.01) |

then used figs 10(a) and (d) of Rozanski & Rowan-Robinson (1994) to estimate the distance modulus for each calibration. The resulting distance moduli are listed in Table 12, where the errors are the combined errors from Rozanski & Rowan-Robinson (1994, table 5), the error in the brightest supergiants magnitude and an error for the host galaxy reddening. We have also included an extra error of 0.5, to account for the transformation of the $I$ magnitudes. A weighted average gives $\mu = 29.44 \pm 0.48$ corresponding to a distance of $D = 7.7 \pm 1.7$ Mpc. Had we excluded the RSG result in light of the warnings of Rozanski & Rowan-Robinson (1994), the distance modulus would be $\mu = 29.31 \pm 0.72$ or $D = 7.3 \pm 2.4$ Mpc. The distance we find is consistent with those of Sohn & Davidge (1996, $D = 7.2$ Mpc) and Sharina et al. (1996, $D = 7.8$ Mpc).

It is interesting however to note that Sharina et al. (1996) use the calibrations of Karachentsev & Tikhonov (1994), which are different to those of Rozanski & Rowan-Robinson (1994). Karachensev & Tikhonov find three different calibrations, two for BSGs and one for RSGs. These are shown in equations (4)–(6), with a standard deviation of $\sigma(M) = 0.30$, 0.30 and 0.45, respectively:

$$\langle M_V \rangle = 0.19 M_B^{\rm gal} - 4.52, \tag{4}$$

$$\langle M_B \rangle = 0.35 M_B^{\rm gal} - 2.50, \tag{5}$$

$$\langle M_B \rangle = -0.51(B - B^{\rm gal}) - 4.14. \tag{6}$$

The distance modulus can be calculated from equations (4) and (5) using an iterative approach starting with the absolute magnitude from Shostak & van der Kruit (1984, $M_B^{\rm gal} = -20.23$). Using this method, we found the distance moduli to be $\mu(V) = 29.71 \pm 0.77$ and $\mu(B) = 30.12 \pm 0.59$, where the errors are the combined errors of the relationship, the error in the magnitude of the brightest supergiants and the reddening of the galaxy, which were both discussed previously. Sharina et al. (1996) used only the calibration given in equation (6) for BSGs, which does not suffer from distance degeneracy. The authors found only one star red enough to be an RSG, but concluded it was a foreground star because of its magnitude. The distance modulus calculated from this relationship is $\mu(B) = 30.11 \pm 0.67$. A mean using the first two relationships only gives a distance modulus of $\mu = 29.91 \pm 0.49$ corresponding to a distance of $D = 9.6 \pm 2.2$ Mpc. This is a difference of 1.9 Mpc using the same data, but with two different calibrations.

### 4.3 Summary and discussion of distance estimates

A summary of distances to M74 from three different methods is listed in Table 13. As well our SCM and brightest supergiants distance estimates, derived in Section 4.1 and 4.2 respectively, we have collated three kinematic and two other brightest supergiants distance estimates from the literature. The kinematic distances shown in the table, use the heliocentric velocity of 656 km s$^{-1}$ and apply three different models of infall onto the Virgo cluster. The values have been corrected for a Hubble constant of $H_0 = 72$ km s$^{-1}$ Mpc$^{-1}$. The simple mean of these distances is also listed in the table, where the

**Table 13.** Summary of distance estimates.

| Method | Source | Distance (Mpc) | Mean |
|---|---|---|---|
| SCM | 1 | 9.6(2.8) | 9.6(2.8) |
| Brightest supergiants | 1 | 7.7(1.7) | 8.1(2.3) |
| | 1 | 9.6(2.2) | |
| | 2 | 7.2(2.0) | |
| | 3 | 7.8(1.6) | |
| Kinematic | 4 | 10.1 | 10.2(2.6) |
| | 5 | 11.1 | |
| | 6,7 | 9.5 | |
| Mean | | | 9.3(1.8) |

(1) This paper, (2) Sohn & Davidge (1996), (3) Sharina et al. (1996), (4) Tully (1988), (5) Ferguson, Gallagher & Wyse (1998), (6) Theureau et al. (1998), (7) http://leda.univ-lyon1.fr.

error is a combination of the error on the mean and the uncertainty resulting from the cosmic thermal velocity dispersion of 187 km s$^{-1}$ (Tonry et al. 2000). The accuracy of these kinematic distances is limited not only by the observed velocity dispersion around the Hubble flow, but on an accurate model to account for the infall onto Virgo and the Great Attractor. Depending on the model, the values range from 9.5–11.1 Mpc, which is a 17 per cent difference, hence there is a large uncertainty associated with this method.

The brightest supergiants distances listed in Table 13 come from three different sources. The first two distances, $D = 7.7 \pm 1.7$ and $9.6 \pm 2.2$ Mpc, are derived in Section 4.2. The third, $D = 7.2 \pm 2.0$ Mpc, is the result of Sohn & Davidge (1996), where the error is a combination of the error in the size of the authors' bin and the error associated with the calibration used (Rozanski & Rowan-Robinson 1994, fig. 10a). The fourth, $D = 7.8 \pm 1.6$ Mpc, is from Sharina et al. (1996), where the error is the combined error associated with the relationship used (Karachentsev & Tikhonov 1994) and the magnitude of the brightest BSGs. The simple mean is also listed in Table 13, where the error is a combination of the statistical error and the systematic error of $\Delta\mu = 0.59$, which corresponds to a distance of 2.2 Mpc (Karachentsev & Tikhonov 1994; Rozanski & Rowan-Robinson 1994). Although the error in the average distance is the lowest of the three methods, the estimates range from 7.2–9.6 Mpc, which is a 26 per cent difference. There are large systematic uncertainties associated with this method and the derived distance also appears to be calibration dependent.

Rozanski & Rowan-Robinson (1994) re-examine most of the existing observational data and investigate claims that the luminosity of the brightest BSGs exhibits a dependence on parent galaxy luminosity, introducing a distance degeneracy. Not only do they confirm this, a similar dependence is also found for the brightest RSGs, which were previously thought to be independent of galaxy luminosity. Rozanski & Rowan-Robinson also find that the resulting error in the distance modulus from this method is far greater than previously believed. Whatever calibration they used, the error in the distance modulus was found never to be less than 0.55 mag. Piotto, Capaccioli & Bresolin (1992) and Karachentsev & Tikhonov (1994) also find such dependencies but find a smaller error in the regression of 0.30 mag. Rozanski & Rowan-Robinson (1994) conclude that this method should not be used in determining the distance to single galaxies. Besides these calibration problems, this method also suffers from crowding, misidentification of supergiants with H II regions, foreground stars, unresolved clusters and OB associations.

**Table 14.** Summary of coefficients from Piotto et al. (1992), Karachentsev & Tikhonov (1994) and Rozanski & Rowan-Robinson (1994) for $M = aM_B^{\rm gal} + b$.

| $M$ | a | b | $\sigma$ ($M$) | Source |
|---|---|---|---|---|
| $M(V)$ | 0.21 | −4.01 | $\gtrsim$0.3 | 1 |
| | 0.19 | −4.52 | 0.30 | 2 |
| | 0.21 | −4.10 | 0.58 | 3 |
| $M(B)$ | 0.36 | −2.29 | ∼0.56 | 1 |
| | 0.35 | −2.50 | 0.30 | 2 |
| | 0.28 | −3.45 | 0.90 | 3 |

(1) Piotto et al. (1992), (2) Karachentsev & Tikhonov (1994), (3) Rozanski & Rowan-Robinson (1994).

These problems associated with poor resolution cause the distance to be systematically underestimated. This is illustrated by Leonard et al. (2003) who derive a Cepheid distance to NGC 1637 that is 50 per cent larger than the brightest RSGs distance estimate of Sohn & Davidge (1998).

The estimates from this paper use *HST* photometry, which has much better resolution than ground based observations and should resolve individual stars from H II regions and compact clusters, reducing this systematic error. If this systematic error is present, we should find larger distances, which is what is found using the calibrations of Karachentsev & Tikhonov (1994). Although our first estimate is comparable to both Sharina et al. (1996) and Sohn & Davidge (1996), our second estimate using a different relationship differs by 2 Mpc. It is worth noting that whereas we have used all four of the calibrations of Rozanski & Rowan-Robinson (1994), Sohn & Davidge (1996) have used just that of fig. 10(a) for RSGs. If we look at the individual estimates of $\mu$ in Table 12, we see that $\mu(a) = 29.70$ is consistent with our results using Karachentsev & Tikhonov, whereas our other results, $\mu(c \rightarrow f)$, are not. If we use the parameters employed by Sharina et al. (1996) to calculate the distance modulus of M74, using the alternative relationships of Rozanski & Rowan-Robinson (1994, fig. 10c), we find $\mu = 28.92$ instead of their $\mu = 29.3$, which is a difference of 1.2 Mpc. Table 14 shows the coefficients of the relationship $M = aM_B^{\rm gal} + b$, found by each of the two different sources plus a third from Piotto et al. (1992). The coefficients of the relationship for RSGs, $M(V)$, are consistent, but when we consider those of the BSGs relation, $M(B)$, there is a disagreement between that of Rozanski & Rowan-Robinson (1994) and the other two papers. Rozanski & Rowan-Robinson find a much shallower relation resulting in the discrepancy between distance moduli. Given the agreement between the coefficients, we consider the larger distance modulus to be more realistic.

The SCM distance estimate also has its uncertainties. This method requires data at a phase of 50 d, which are not always available. In order to obtain the necessary photometric data, Hamuy (2004a) interpolated the observed $V$ and $I$ magnitudes to 50 d post-explosion. In most cases, the author was also able to interpolate the velocities by fitting a power law to the observed velocities (Hamuy 2001), to an accuracy of $\pm$ 300 km s$^{-1}$. In four cases though, it was necessary to extrapolate, introducing an error of 2000 km s$^{-1}$. The redshifts used in Hamuy (2004a) were derived from the observed heliocentric redshifts and converted to the cosmic microwave background frame in order to remove their peculiar motion. This in itself is limited by the accuracy of the model and by the cosmic thermal velocity. Hamuy noted that the least satisfactory aspect of the SCM is the dereddening method based on the comparison of SN colour curves, which yields different results depending on what colour is used. It also depends on the accuracy of the reddening determination of the model SN. Whilst not as accurate as distances derived from SN Ia, the SCM does give distances to within 15 per cent. This method also gives comparable values of $H_0$ to those of Freedman et al. (2001).

In Section 3.3, we highlighted the difficulties in measuring the minimum of the blueshifted trough of the Fe II λ5169 line at later epochs. We found this was not as much of an issue at earlier epochs where the velocity is needed for the SCM. A large uncertainty however was introduced in our application of the SCM, as a result of our lack of data at 50 d. Although this is the case, we have been conservative in our error analysis and the SCM distance of $D = 9.6 \pm 2.8$ Mpc is consistent with other distance estimates and associated errors.

Each of the three different methods to measure distance have similar uncertainties and all have shortcomings. We have therefore taken an unweighted mean of the results of each method to give an absolute distance of $D = 9.3 \pm 1.8$ Mpc, where the error is the error on the mean.

## 5 ESTIMATE OF EJECTED $^{56}$NI MASS

The comparison of the light curve of SN 2003gd with that of SN 1999em in Fig. 4 highlighted a major difference between the two SNe. The lower tail luminosity was attributed to a smaller amount of nickel synthesized in the explosion as was also suggested by Van Dyk et al. (2003). Here, we use three different methods to ascertain the mass of $^{56}$Ni produced. It was first of all estimated using the method of Hamuy (2003), secondly using a direct comparison with the light curve of SN 1987A and lastly using the new though unconfirmed method of Elmhamdi, Chugai & Danziger (2003a).

### 5.1 Nickel mass from the bolometric luminosity of the exponential tail

Hamuy (2003) derives $M_{\rm Ni}$ from the bolometric luminosity of the exponential tail, assuming that all of the $\gamma$-rays resulting from $^{56}{\rm Co} \rightarrow {}^{56}{\rm Fe}$ decay are fully thermalized. We first convert our $V$-band photometry in the tail to bolometric luminosities using the formula given in equation (1) of Hamuy (2003), which is given here in equation (7). The bolometric correction is $BC = 0.26 \pm 0.06$ and the additive constant converts from Vega magnitudes to cgs units (Hamuy 2001, 2003). We have used the distance derived in Section 4.3:

$$\log\left(\frac{L}{\rm erg\ s^{-1}}\right) = \frac{-(V - A_V + BC) + 5\log D - 8.14}{2.5}, \qquad (7)$$

$$M_{\rm Ni} = 7.866 \times 10^{-44} L \exp\left[\frac{(t - t_0)/(1 + z) - \tau_{\rm Ni}}{\tau_{\rm Co}}\right] {\rm M}_\odot. \qquad (8)$$

The nickel mass was then found using equation (2) of Hamuy (2003) given here in equation (8), where $t_0$ is the explosion epoch, $\tau_{\rm Ni} = 6.1$ d is the half-life of $^{56}$Ni and $\tau_{\rm Co} = 111.26$ d is the half-life of $^{56}$Co. Using this method, we estimated $M_{\rm Ni}$ for each of the points in the tail and by taking a simple average of these we found $M_{\rm Ni} = 0.016^{+0.019}_{-0.008}\,{\rm M}_\odot$. This is approximately a third of that produced in SN 1999em, hence the lower tail luminosity. There is a large uncertainty associated with this value as the nickel mass calculation is strongly dependent on the explosion time, extinction and the distance, all of which are not well known. We have therefore calculated the range of nickel masses, for each point, from the extreme values for each parameter in equations (7) and (8). We have

taken an average of the maximum and minimum values and have estimated a more appropriate error from these.

### 5.2 Nickel mass from a direct comparison to the SN 1987A light curve

The $^{56}$Ni mass was also estimated from the difference in the UVOIR light curves of SN 2003gd and SN 1987A, assuming the same $\gamma$-ray deposition. A $\chi^2$-fitting algorithm was used to shift the light curve of SN 1987A onto that of SN 2003gd to find the best fit. When constructing the light curve of SN 1987A, a distance of 50 kpc was adopted. The difference in log luminosity was found to be $\log(L^{87A}/L) = 0.664 \pm 0.193$. Equation (9) was then used to scale the nickel mass of SN 1987A, which was taken to be 0.075 $M_\odot$ (e.g. Turatto et al. 1998), to estimate that of SN 2003gd:

$$M_{\rm Ni} = 0.075 \times \left(\frac{L}{L^{87A}}\right) {\rm M}_\odot. \quad (9)$$

Using this method, we find $M_{\rm Ni} = 0.016 \pm 0.008\,{\rm M}_\odot$, where the error is the error associated with the fit combined with an error of $0.003\,{\rm M}_\odot$ related to the uncertainty in the explosion date. This method is however still dependent on the distance to the SN, although the error in the nickel mass amply accounts for this.

### 5.3 Nickel mass from the 'steepness of decline' correlation

Elmhamdi et al. (2003a) reported a correlation between the rate of decline in the $V$ band, from the plateau to the tail, and the nickel mass estimated from the SN 1987A method. The authors defined a steepness parameter, $S$, which is the maximum gradient during the transition in mag d$^{-1}$. A sample of 10 SNe II-P were used in determining the best linear fit, which is given in equation (10):

$$\log\left(\frac{M_{\rm Ni}}{{\rm M}_\odot}\right) = -6.2295S - 0.8147. \quad (10)$$

The steepness parameter for SN 2003gd was found to be 0.25, which yields the rather low result of $M_{\rm Ni} = 0.004^{+0.002}_{-0.001}\,{\rm M}_\odot$. The error was estimated from the scatter around the linear fit in the log $(M_{\rm Ni}/{\rm M}_\odot)/S$ plane, $\log(M_{\rm Ni}/{\rm M}_\odot) = 0.147$, and equation (10) was used to translate this into a mass. This error is probably much larger as a result of the error in the fit.

### 5.4 Discussion of the nickel mass estimate

The three independent methods, to obtain nickel mass, give two concurrent results of $0.016\,{\rm M}_\odot$ and one rather low estimate of $0.004\,{\rm M}_\odot$. The first two methods are both dependent on the explosion date and the distance, although the errors sufficiently accommodate these. The method of Hamuy (2003) assumes that the $\gamma$-rays are fully thermalized, but as the slope of the exponential tail of SN 2003gd follows the decay of $^{56}$Co, this is not unreasonable. The direct comparison to the light curve of SN 1987A assumes that SN 2003gd deposited a similar fraction of $\gamma$-rays as SN 1987A. As the late-time decline of SN 1987A was very close to the decay rate of $^{56}$Co, this assumption is also not unfounded. The method of Elmhamdi et al. (2003a) has the advantage of being independent of explosion epoch and distance, although it is an unconfirmed method. The correlation itself is distance dependent and relies on the SN 1987A method. The result is very low and would suggest that the adopted distance of 9.3 Mpc is out by a factor of 2, which is unlikely. Given that the first two results are concurrent and the errors adequately reflect the uncertainties, we take the average of the first two results and estimate a nickel mass of $M_{\rm Ni} = 0.016^{+0.010}_{-0.006}\,{\rm M}_\odot$.

## 6 MODEL COMPARISON

We compared the data of SN 2003gd with the output of a semi-analytic light curve code (see Zampieri et al. 2003, for a detailed description of the code and the adopted initial conditions). The goal of this comparison is twofold. First of all, we want to put some constraints on the input parameters (in particular the opacity) of the semi-analytic code by checking to see whether the mass estimate from the code is consistent with the observed measurement of the progenitor mass of $8^{+4}_{-2}\,{\rm M}_\odot$ (Smartt et al. 2004). Secondly, we would also like to use the code to derive some limits on the SN distance and explosion date, which are rather uncertain. The code performs an estimation of the ejected envelope parameters from a simultaneous comparison of the observed and computed light curve, photospheric gas velocity and continuum temperature. The main input parameters of the envelope are listed in Table 15. The fraction of the initial energy that goes into kinetic energy and the colour correction factor (that measures the deviation of the continuum radiation temperature $T_{\rm c}$ from the blackbody effective temperature $T_{\rm eff}$) are input constants and are fixed at the values 0.5 and 1.2, respectively. An important physical quantity that must be specified and that may affect in a significant way theoretical mass estimates is the envelope gas opacity $\kappa$.

The parameters of the model fits, corresponding to different choices of the explosion epoch and distance, are reported in Table 15, where the estimated error in the parameters is ∼20–30 per cent. For models A and B, we assume that the phase identification derived in Section 3.1 is correct, implying that the explosion epoch is JD 245 2717 (86 d before discovery). The two models differ in the adopted SN distance, $D = 7.3$ Mpc for model A and $D = 9.2$ Mpc for model B. Model C assumes JD 245 2737 (∼65 d before discovery) for the explosion epoch and $D = 7.3$ Mpc for the distance.

The results for model A are shown in Fig. 18. The overall agreement with the observed light curve, photospheric gas velocity and continuum temperature is rather good. The data are reproduced by a slightly underenergetic explosion ($E = 1.4 \times 10^{51}$ erg) that has ejected $M = 11\,{\rm M}_\odot$ and $M_{\rm Ni} = 9 \times 10^{-3}\,{\rm M}_\odot$. The comparison

**Table 15.** Theoretical parameters of SN 2003gd from the semi-analytic model of Zampieri et al. (2003).

| | $R_0$ ($10^{13}$ cm) | $M$ ($M_\odot$) | $M_{\rm Ni}$ ($M_\odot$) | $V_0$ ($10^8$ cm s$^{-1}$) | $E$ ($10^{51}$ erg) | $\kappa$ (cm$^2$ g$^{-1}$) | $t_{\rm rec,0}$ (days) | $T_{\rm eff}$ (K) |
|---|---|---|---|---|---|---|---|---|
| Model A | 2.3 | 11 | $9 \times 10^{-3}$ | 3.2 | 1.4 | 0.34 | 45 | 4600 |
| Model B | 2.7 | 13 | $1.5 \times 10^{-2}$ | 3.4 | 1.8 | 0.34 | 40 | 5000 |
| Model C | 2 | 6 | $7 \times 10^{-3}$ | 3.2 | 0.7 | 0.34 | 45 | 4600 |

$R_0$ initial radius of the ejected envelope; $E$ initial thermal + kinetic energy of the ejecta; $M$ ejected envelope mass; $\kappa$ gas opacity; $M_{\rm Ni}$ ejected $^{56}$Ni mass; $t_{\rm rec,0}$ time when the envelope starts to recombine; $V_0$ velocity of the envelope at the outer shell; $T_{\rm eff}$ effective temperature during recombination.

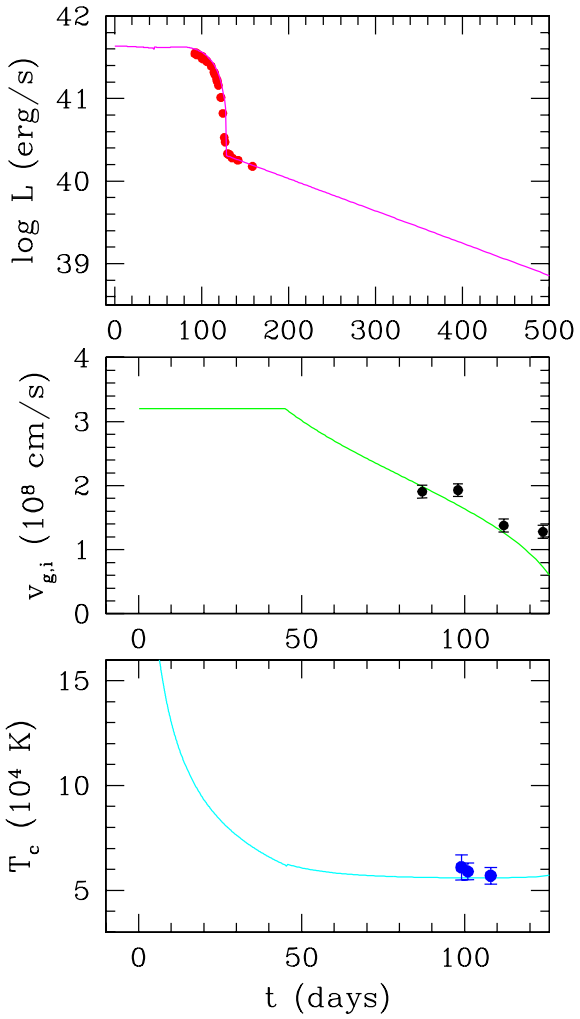


**Figure 18.** Results for model A showing $V$-band luminosity, $L$, velocity of metal (Sc II λ 6246) lines, $v_{g,i}$, and continuum temperature, $T_c$, as a function of time for SN 2003gd. The adopted distance modulus and the estimated total reddening are $\mu = 29.32$ and $A_V = 0.42$. The assumed explosion date is JD 245 2717. The solid lines represent the curves from the semi-analytic model of Zampieri et al. (2003).

of the inferred value of $M$ and the observed measurement of the progenitor mass shows that the star was probably in the upper end of the estimated mass range and sets an interesting constraint on the average opacity of the ejected envelope gas. In fact, values of $\kappa \leqslant 0.3$ cm$^2$ g$^{-1}$ result in ejected envelope masses in excess of 11 M$_\odot$, barely consistent with the progenitor mass estimated from direct pre-explosion observations, once the compact remnant mass is taken into account (Smartt et al. 2004). Thus, large opacities are needed, in the range $\kappa = 0.3 - 0.4$ cm$^2$ g$^{-1}$ ($\kappa = 0.34$ cm$^2$ g$^{-1}$ in Fig. 18). Opacities in this range are appropriate for an envelope comprising mostly hydrogen, with a composition close to solar. This suggests that little mixing has occurred in SN 2003gd, the helium and other elements synthesized during nucleosynthesis remaining buried beneath the envelope.

Model B tests the agreement between the model and the data assuming a different SN distance. This model has a rather typical explosion energy ($E = 1.8 \times 10^{51}$ erg), while the ejected Ni mass ($M_{\rm Ni} = 1.5 \times 10^{-2}$ M$_\odot$) is approximately 5 times lower than the average value for a normal SN II-P ($M_{\rm Ni} = 7.5 \times 10^{-2}$ M$_\odot$). We note, however, that there is evidence to suggest a continuous distribution of $M_{\rm Ni}$ in SNe II-P (see Fig. 23). The ejected envelope mass in this model is $M = 13$ M$_\odot$. Considering the mass of the compact remnant, this result indicates that $M$ may be too large to be consistent with a progenitor of $\leqslant$12 M$_\odot$. Therefore, if the phase of the SN at discovery is ∼90 d, the distance should be probably lower than 9 Mpc, in the lower end of the estimated range of distances.

The uncertainty in the explosion epoch, however, is rather large and it cannot be ruled out that the discovery epoch is actually closer to the explosion date than estimated. Model C was run to test this possibility. We find that the data of SN 2003gd are reproduced by a fairly low energy explosion ($E = 0.7 \times 10^{51}$ erg) with the ejection of 6 M$_\odot$ and a small amount of Ni ($M_{\rm Ni} = 7 \times 10^{-3}$ M$_\odot$). In this case, smaller values of the opacity and/or larger distances would make the model still in agreement with the observations. However, an event of this type would have a plateau lasting $\leqslant$90 d, which is shorter than what is commonly observed in SNe II-P. Furthermore, the theoretical photospheric gas velocity appears to overestimate significantly (>20 per cent) the observed line velocity at discovery.

## 7 DISCUSSION

### 7.1 SN 2003gd: a typical Type II-P supernova?

Unfortunately, SN 2003gd was discovered ∼86 d after explosion (Section 3.1) when it appeared from behind the sun. Because valuable information about this SN was lost, we have made various assumptions about the SN based on the striking spectroscopic similarities with SN 1999em and their comparable progenitor masses. Although SN 2003gd is spectroscopically very similar to SN 1999em, it is fainter in its tail luminosity as a result of the lower nickel mass synthesized in the explosion. Hamuy (2003) presented evidence to suggest that the plateau luminosities and velocities are correlated with the amount of nickel produced (see also Fig. 23). The lower tail luminosity may therefore suggest that SN 2003gd was intrinsically much fainter than SN 1999em, although the spectral similarities and velocities at the end of the plateau phase would suggest otherwise. A number of papers have recently featured peculiar low-luminosity, low-nickel SNe II-P (e.g. Zampieri et al. 2003; Pastorello et al. 2004a,b), but the question is, could SN 2003gd also belong to that group and, if so, were our earlier assumptions justified?

Elmhamdi et al. (2003a) and Pastorello et al. (2004b) noted a rapid excess in the $(B - V)$ and $(V - R)$ colours of the low-luminosity, or faint, SN 1997D at the end of the photospheric phase (see Fig. 19). This behaviour was also observed by Pastorello et al. (2004b) in SN 1999eu, another faint SN, in the form of a sharp spike. Pastorello et al. suggested that the excess in colour may be characteristic of this low-luminosity subgroup. Fig. 19 shows the intrinsic colour curves of SN 2003gd alongside those of the prototypical peculiar faint SN 1997D (Turatto et al. 1998; Benetti et al. 2001; Pastorello et al. 2004a) and the model normal SN 1999em. The $(B - V)_0$ colour curve of SN 2003gd does rise more rapidly than that of SN 1997D, but it does not reach a significant excess. The SN 2003gd colours of Van Dyk et al. (2003) also do not display this steeper rise. The $(V - R)_0$ colour evolution of SN 2003gd is slightly more rapid than that of SN 1999em, at the end of the plateau phase, but it is nearer to the evolution of the normal SN. There may be a small spike in the colour of SN 2003gd at the end of the plateau phase at around 120 d, but the photometry is sparse and it is therefore difficult to confirm its existence. We would also note that there may also be a slight peak in the colour curve of SN 1999em at ∼8 d later. From these colour evolutions, SN 2003gd appears to be more like a normal SN

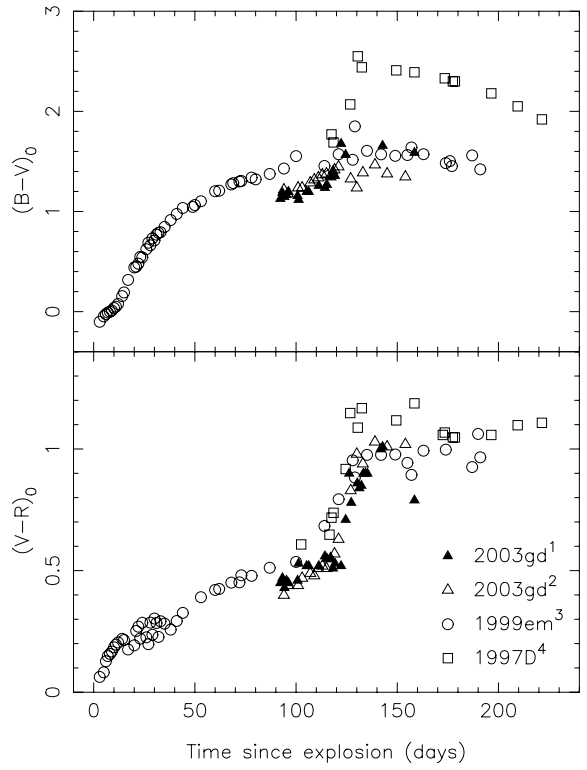


**Figure 19.** Intrinsic ($B - V$) and ($V - R$) colour curves of SN 2003gd alongside those of the prototypical peculiar, faint SN 1997D and the normal SN 1999em. The superscripts in the figure denote the source of the photometry: (1) this paper, (2) Van Dyk et al. (2003), (3) Hamuy et al. (2001) and (4) Benetti et al. (2001).

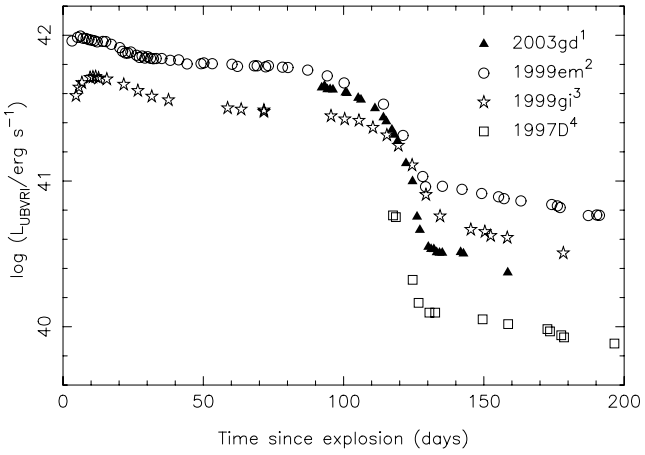


**Figure 20.** Comparison between the UVOIR light curves of SNe 2003gd, 1999em, 1999gi and 1997D, which have nickel masses of 0.016, 0.048, 0.022 and 0.006 $M_{\odot}$, respectively. The nickel masses for SNe 1999em and 1999gi are from Hamuy (2003), and the nickel mass for 1997D is from Pastorello et al. (2004b), which are corrected for the revised distances used here. The superscripts in the figure denote the source of the photometry: (1) this paper, (2) Hamuy et al. (2001), (3) Leonard et al. (2002b) and (4) Benetti et al. (2001).

II-P. In order to further investigate our assumptions, we compared the UVOIR light curves and spectra of SN 2003gd with examples of normal and faint SNe II-P.

The UVOIR light curve of SN 2003gd is shown in Fig. 20 along with those of three other SNe II-P, SNe 1999em, 1999gi and 1997D,

**Table 16.** Distance estimates of NGC 3184 found in literature.

| Method | Source | Distance (Mpc) | Mean |
|---|---|---|---|
| Tully-Fisher | 1 | 14.9 | 11.1 |
| | 2 | 7.2 | |
| Tertiary indicators | 3 | 7.9 | 7.9 |
| EPM | 4 | 11.1 | 11.1 |
| Kinematic | 1 | 10.6 | 9.9 |
| | 5 | 9.1 | |
| Mean | | | $10.0 \pm 0.8$ |

(1) http://leda.univ-lyon1.fr, (2) Pierce (1994), (3) de Vaucouleurs (1979), (4) Leonard et al. (2002b), (5) Tully (1988).

where SN 1999gi is a normal plateau event. These UVOIR light curves were calculated by summing up all the contributions from the *UBVRI* observations of each SN. The few observations in *U* were used to estimate the contribution to the total flux from that band. In the case of SN 1999gi, where there was no *U*-band photometry, the *U*-band contribution was taken to be the same as that for SN 1999em. The distances used to calculate the UVOIR light curves were $11.4 \pm 0.9$, $10.0 \pm 0.8$ and $15.3 \pm 1.9$ Mpc for SNe 1999em, 1999gi and 1997D, respectively. The distance used for SN 2003gd is that discussed in Section 4.3. The distance of SN 1999em used here is the straight average of those discussed by Leonard et al. (2003, Table 9). The distance of SN 1999gi, the host galaxy of which was NGC 3184, was taken to be the simple mean of the distance estimates found in the literature, which are summarized in Table 16 where the error is the error on the mean. A literature search for the host galaxy of SN 1997D, NGC 1536, returned two kinematic distances, 14.0 and 16.7 Mpc, from Tully (1988) and the Lyon-Meudon Extragalactic Database (LEDA) which yield an average of $15.3 \pm 1.3$ Mpc. All kinematic distances were corrected for a Hubble constant of $H_0 = 72\,\mathrm{km\,s^{-1}\,Mpc^{-1}}$. The plateau luminosity of SN 2003gd is similar to that of SN 1999em at the end of the plateau, but dips to below both SNe 1999em and 1999gi during the tail phase. Although the decline from the plateau to the tail is greater and steeper in SN 2003gd than in the normal SNe II-P, the tail luminosity is much brighter than that of the faint, nickel-poor SN 1997D.

The spectrum of SN 2003gd at 100 d is compared to the spectra of SNe 1999em and 1997D at a similar phase, in Fig. 21. The spectra have been flux scaled using the method of Section 2.2, with the spectra of 1997D being scaled by an extra factor of 5 for clarity. The spectrum of SN 2003gd shows some similarities to both SNe 1997D and 1999em, but more so to that of SN 1999em with its broad spectral features. The spectral flux of SN 1997D is much fainter than that of SN 2003gd and also has much narrower spectral features indicative of the lower velocities. The appearance of the spectra, the higher velocities, the colour evolution and higher plateau luminosities of SN 2003gd suggest that it is more akin to the normal Type II-P events.

### 7.2 Implications for the progenitor of SN 2003gd

Smartt et al. (2004) present the discovery of the RSG that exploded as SN 2003gd. The galaxy was imaged 6 to 9 months before the SN explosion by the *HST* and the Gemini Telescope. *HST* images after the explosion confirmed the positional coincidence of the SN with a single resolved star. The observational properties of the star were compared with stellar evolutionary tracks. The colours and luminosity of the progenitor star were found to be consistent with those of

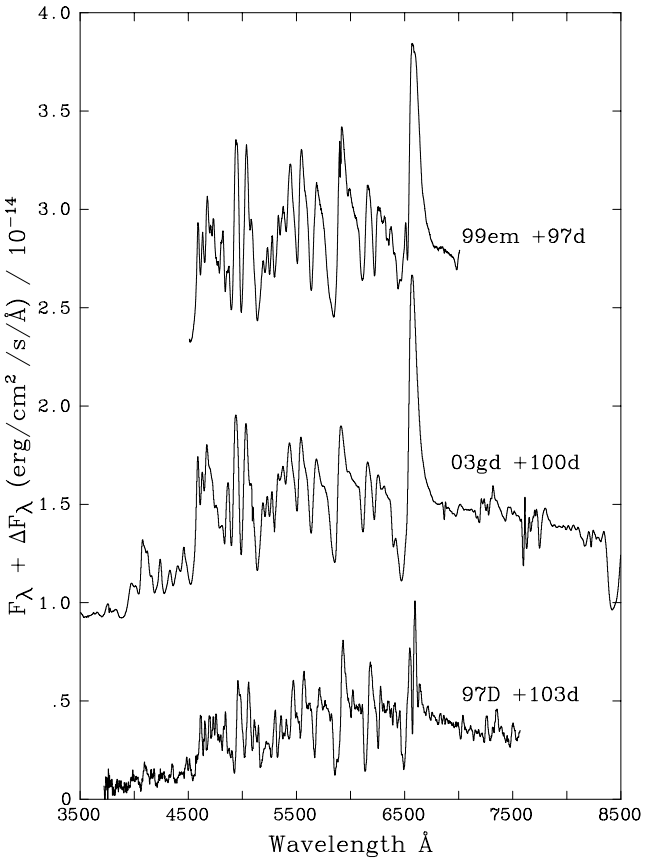


**Figure 21.** Comparison between the spectra of SNe 2003gd, 1999em and 1997D, which have nickel masses of 0.016 $M_\odot$, 0.048 $M_\odot$ (Hamuy 2003) and 0.006 $M_\odot$ (Pastorello et al. 2004b), respectively, corrected for the distances used in this paper. SNe 1999em and 1997D are representative of a normal and a faint Type II-P supernova (SN II-P), respectively.

an RSG with an initial main-sequence mass of $8^{+4}_{-2}\,M_\odot$. However, the reddening and distance used in Smartt et al. (2004) has since been updated to $A_V = 0.43 \pm 0.19$ (Section 3.2) and $D = 9.3 \pm 1.8$ (Section 4.3), and we recalculate the bolometric luminosity of the progenitor star using these values. We find $M_{\rm bol} = -6.0 \pm 0.7$ with no difference in the corresponding luminosity of log $(L/L_\odot) = 4.3 \pm 0.3$. We therefore find no changes to the authors' conclusions.

We use equation (2) of Nadyozhin (2003), shown here in equation (11),

$$\log\left(\frac{M_{\rm ej}}{M_\odot}\right) = 0.234 M_V + 2.91 \log\left(\frac{\Delta t}{\rm days}\right) + 1.96 \log\left(\frac{u_{\rm ph}}{10^3\ {\rm km\ s^{-1}}}\right) - 1.829, \quad (11)$$

to compare the observed properties of SN 2003gd with the observed mass of $8^{+4}_{-2}\,M_\odot$. Because we can only make assumptions about the length of the plateau, we have used this equation to constrain the plateau length to ascertain whether it is consistent with other SNe II-P. Based on the observed mass, we have estimated the ejected mass to be $6\,M_\odot$, leaving $2\,M_\odot$ for the mass of the compact remnant plus other mass losses from the system. We find that the observed mass is consistent with a plateau length of $67^{+34}_{-25}$ d, where the errors are the combined errors in each of the parameters in the equation. For the error in the ejected mass we have added, in quadrature, an extra error of $1\,M_\odot$ to the error in the observed mass. Using the full range of the observed mass and other parameters, we find the SN parameters are consistent with a plateau range of 40–119 d, although realistically this is unlikely to be below around 90 d, from what is commonly observed for SNe II-P. Within the errors, this mass appears not to be inconsistent with the observations and may suggest a mass in the upper end of the mass range.

The model of Zampieri et al. (2003), when applied to SN 2003gd (see Section 6), also seems to favour a main-sequence mass in the upper end of the observed range, although this is achieved with a distance in the lower end of our distance range (model A). Model B estimates an ejected mass of $13\,M_\odot$ using 9.2 Mpc, so is directly comparable with the observed mass. This is just outside the observed mass range, but is not necessarily inconsistent given the theoretical uncertainties associated with the model. The model does appear to rule out an explosion date closer to discovery (model C). We would like to stress though that more observations of progenitors are needed to fully test and constrain this model.

The observations of progenitors have important implications for the low-luminosity, faint SNe II-P. There are two very different plausible progenitor models for these, one being the low-energy explosion of massive stars (e.g. Turatto et al. 1998; Benetti et al. 2001; Zampieri et al. 2003). In this model the collapsing core forms a black hole and a significant amount of fall-back of material occurs. An alternative scenario is the low-energy explosion of low-mass stars, presented by Chugai & Utrobin (2000) who successfully reproduced the observations of SN 1997D with an explosion of $10^{50}$ erg and an ejected mass of $6\,M_\odot$. The findings of Zampieri, Ramina & Pastorello (2004) support the high-mass progenitor scenario. The authors find a bimodal distribution of SNe in the nickel mass, initial main-sequence mass ($M_{\rm MS}$) plane. A reproduction of the authors' fig. 1 (right) is shown here in Fig. 22 with the observational points of SNe 2003gd and 1999em added with filled circles. Zampieri remarks that the theoretical estimates of $M_{\rm MS}$ from Zampieri et al. (2004), shown with open circles in the figure, will

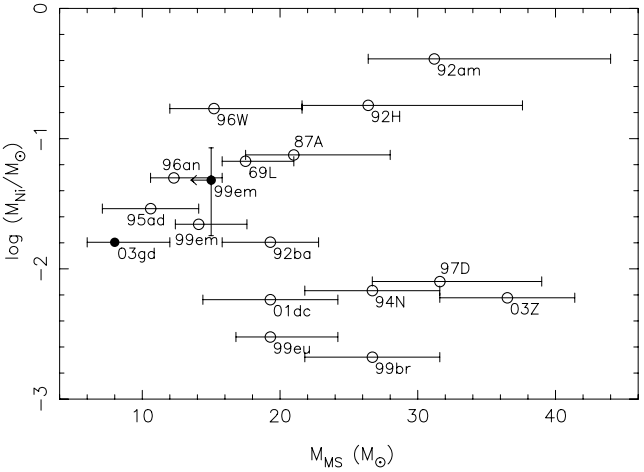


**Figure 22.** Reproduction of fig. 1 (right) of Zampieri et al. (2004) showing the bimodal distribution of SNe II-P, in the $M_{\rm Ni}/M_{\rm MS}$ plane, from their model. The open circles show theoretical data from the semi-empirical model of Zampieri et al. (2003), where $M_{\rm MS}$ is estimated from the ejected envelope mass. The filled circles show observational data for SNe 2003gd and 1999em, where $M_{\rm Ni}$ is estimated from the light curve and $M^{\rm 99em}_{\rm MS}$ is an upper mass limit only (Smartt et al. 2002a). SN 2003gd inhabits the lower end of the normal Type II-P branch.

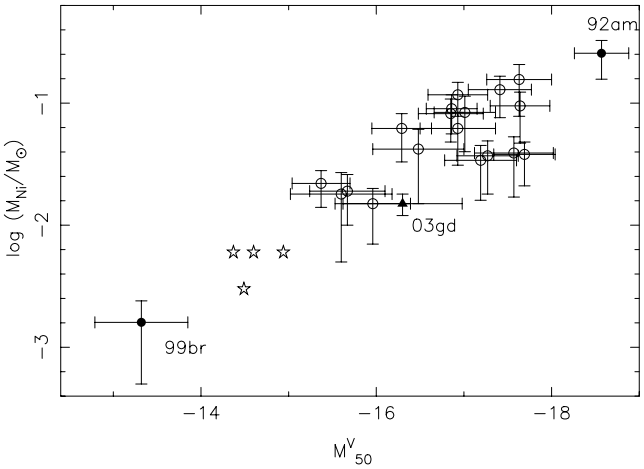


**Figure 23.** Reproduction of fig. 3 of Hamuy (2003) showing the correlation between the mass of $^{56}$Ni synthesized in the SN with the absolute magnitude in the *V* band at 50 d after explosion. The figure has additional points of SN 2003gd, shown with a filled triangle, and four faint SNe, 1994N, 1999eu, 2001dc and 2003Z, shown with open stars, from Pastorello (2003).

most probably need to be revised using the value of the opacity from Section 6. In this picture, the upper branch forms the normal Type II-P branch and the lower the faint branch, with SN 2003gd occupying the lower end of the normal branch. The alternative low-mass scenario positions the faint SNe at the lower end of the normal branch in one continuous distribution. Until there are direct detections of the progenitor stars of these SNe, we cannot determine if either of these models is a true model.

SNe II-P produce a large range of nickel masses from around $10^{-3}$ to $10^{-1}$ $M_{\odot}$. Hamuy (2003) showed that a correlation exists between the amount of nickel produced in the explosion and the absolute magnitude in the *V* band during the plateau phase. A reproduction of Hamuy's fig. 3 is shown here in Fig. 23 with SN 2003gd shown with a filled triangle. Four other SNe, 1994N, 1999eu, 2001dc and 2003Z, represented with open stars, are from Pastorello (2003). These four SNe plus SN 1999br are from the group of faint SNe II-P. In this figure, SN 2003gd is in the centre of a continuous distribution of SNe between the low-nickel, faint SN 1999br and the high-nickel, bright SN 1992am.

Smartt et al. (2003a) made a comparison between all the known, direct information available on SN progenitors with the theoretical predictions of Heger et al. (2003), whose work on the pre-SN evolution of massive stars produced SN population diagrams as a function of mass and metallicity. These models do not consider binary stars or rotation. We plot this SN population diagram in Fig. 24 and add SN 2003gd, which has a solar metallicity (Smartt et al. 2004). We repeat the caution that Smartt et al. issues, emphasizing that at present this is a qualitative comparison. Whilst saying this, the progenitor detected for SN 2003gd is consistent with the theoretical Type II-P region undergoing an O/Ne/Mg core collapse albeit close to the theoretical boundaries.

## 8 CONCLUSIONS

We have presented photometric and spectroscopic data on the Type II-P SN 2003gd. We compared the *BVRI* light curves with those of the well-observed, spectroscopically similar SN 1999em using a $\chi^2$-fitting algorithm. This analysis allowed us to estimate an explosion epoch of JD 245 2717 ± 21, corresponding to a date of 2003 March 18, and the *VI* magnitudes during the plateau phase. It was noted during this analysis that the tail luminosity of SN 2003gd was much lower than that of SN 1999em. Using this explosion epoch, we were able to compare the velocity evolution of SN 2003gd with those of other similar SNe II-P. The velocity evolution was found to be comparable at all epochs in our data set. This enabled us to extrapolate the velocity evolution of SN 2003gd backwards to find the velocity during the plateau phase.

We calculated three distances to M74 using two different methods, the SCM (Hamuy 2003, 2004a,b) and the BSM (brightest supergiants method; Rozanski & Rowan-Robinson 1994; Karachentsev & Tikhonov 1994). First, using the inferred

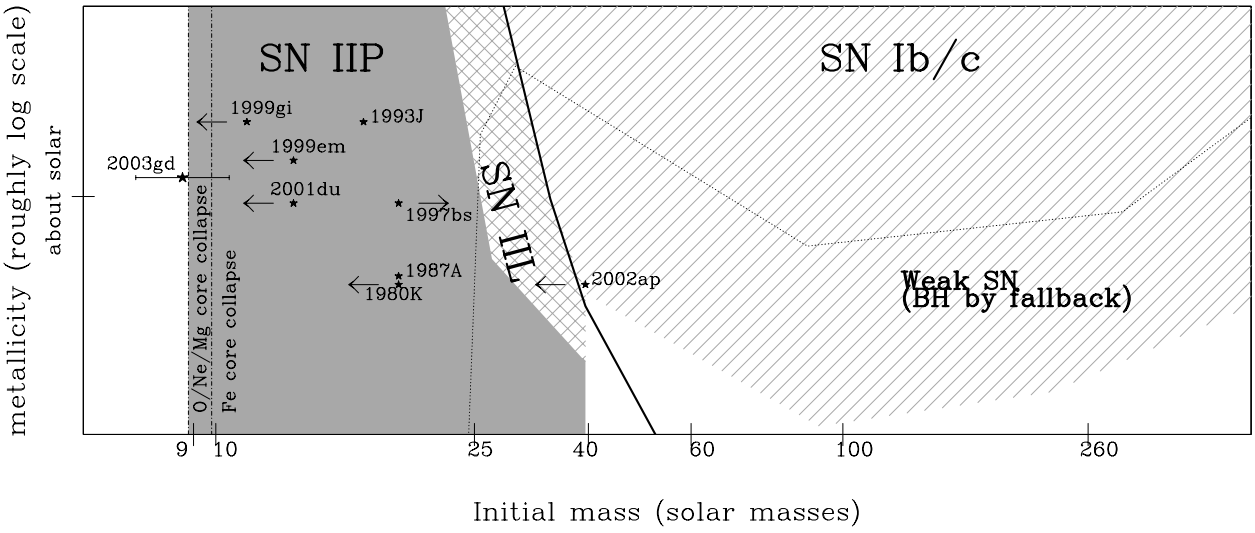


**Figure 24.** Theoretical SNe populations from the models of Heger et al. (2003). All objects below the dotted line should produce low luminosity SNe resulting from black hole formation and subsequent fall-back of material onto the iron core. All objects to the right of the solid black line should have lost their hydrogen envelope by the point of collapse resulting in hydrogen-free SNe. The white regions indicate areas where SNe should not be observed. The observed positions of the SNe are approximately estimated and placed accordingly, where the arrows indicate those with limits. The zero-point on the *y*-axis is assumed to be log $(Z/Z_{\odot}) = -1$.

velocity and $VI$ magnitudes, we estimated a distance of $D = 9.6 \pm 1.8$ Mpc with the SCM. We then used *HST* (WFPC2) photometry to estimate the distances of $7.7 \pm 1.7$ and $9.6 \pm 2.2$ Mpc using two different BSM calibrations. Using these three distances and other distances within the literature, we estimated an overall distance of $9.3 \pm 1.8$ Mpc to M74. This distance allowed the mass of $^{56}$Ni to be estimated at $0.016\,M_{\odot}$.

A comparison was made between the observed data of SN 2003gd and the semi-analytical models of Zampieri et al. (2003). These models first tested the input parameters of the code and secondly ascertained whether the distance and explosion epoch were consistent with the observed progenitor mass. It was found that, in order for the model to produce an ejected mass consistent with the observed progenitor mass, the opacities needed were large, $\kappa = 0.3 - 04$ cm$^{-2}$ g$^{-1}$, suggesting little mixing occurred in SN 2003gd. The results of the models suggested that the progenitor was probably in the upper end of the progenitor mass range of $8^{+4}_{-2}\,M_{\odot}$ and the explosion was not likely to have occurred much later than estimated in Section 3.1.

The low tail luminosity of SN 2003gd sparked a debate about the nature of this SN, whether it was a normal Type II-P or whether it belonged to the group of faint, low-nickel SNe. To ascertain this, we compared the colour evolution, pseudo-bolometric light curve and a spectrum (100 d) of SN 2003gd with those of SNe belonging to the normal and faint groups. We also compared the observed mass of the SN with theoretical models. Using all the information available for SN 2003gd, we conclude the following.

(i) The colour evolution of SN 2003gd is similar to that of the normal SNe II-P. Although the reddening at the end of the plateau phase is slightly steeper, it does not show a colour excess like the faint SNe.

(ii) The plateau luminosity of SN 2003gd is comparable to those of normal SNe II-P, although the decline from the plateau to the tail is greater.

(iii) The tail luminosity of SN 2003gd, despite the larger decrease, is greater than the tail luminosity of the faint SNe II-P.

(iv) The spectra are much more similar to the normal SNe II-P, with their broad spectral features, than the faint SNe, which are much fainter and have much narrower spectral features.

(v) The velocities of SN 2003gd are comparable to those of the normal Type II-P group.

(vi) SN 2003gd lies in the centre of the correlated, continuous distribution of SNe II-P in the $M_{\rm Ni}/M_V$ plane, which has the low-nickel, faint SN 1999br and high-nickel, bright SN 1992am at its extremities.

(vii) The observed progenitor mass of SN 2003gd lies at the lower end of the normal SN II-P branch in the $M_{\rm Ni}/M_{\rm MS}$ plane (Zampieri et al. 2003).

(viii) In the SN population diagram of Heger et al. (2003), the observed progenitor mass of SN 2003gd lies in the Type II-P region, which undergoes O/Ne/Mg core collapse, albeit close to the boundaries.

We therefore conclude that the observations and observed properties of SN 2003gd are consistent with the observed progenitor star, an RSG of mass $8^{+4}_{-2}\,M_{\odot}$ (Smartt et al. 2004), which resulted in a normal SN II-P at the end of its life.

## ACKNOWLEDGMENTS

Observations were made using the William Herschel Telescope (WHT), INT and JKT, which are operated by the Isaac Newton Group (ING), and also with the Italian TNG, which is operated by the Centro Galileo Galilei of the Instituto Nazionale di Astrofisica (INAF). These telescopes are operated on the island of La Palma at the Spanish Observatorio del Roque de los Muchachos of the Instituto de Astrofísica de Canarias. This paper is also partially based on observations collected at the Asiago Observatory, Italy, and at the ESO, Chile. We would like to thank the ING for their rapid response to our service proposal, and D. Lennon and F. Prada for making these observations. We would also like to thank S. Di Tomaso, G. Andreuzzi and the staff at the TNG who contributed to taking the TNG observations and for their excellent support. We would also like to thank F. Patat for obtaining the VLT data. MAH, JRM and SJS would like to thank PPARC for their financial support. S. Leon and S. Verley are partially supported by the Spanish Ministerio de Ciencia y Tecnologia Grant AYA 2002-03338 and SL by an Averroes Fellowship from the Junta de Andalucía.

## REFERENCES

Altavilla G. et al., 2004, MNRAS, 349, 1344
Bahcall J. N., Soneira R. M., 1981, ApJS, 47, 357
Baron E. et al., 2000, ApJ, 545, 444
Belley J., Roy J., 1992, ApJS, 78, 61
Benetti S. et al., 2001, MNRAS, 322, 361
Cardelli J. A., Clayton G. C., Mathis J. S., 1989, ApJ, 345, 245
Chugai N. N., Utrobin V. P., 2000, A&A, 354, 557
Dolphin A. E., 2000a, PASP, 112, 1397
Dolphin A. E., 2000b, PASP, 112, 1383
Drilling J. S., Landolt A. U., 2000, in Arthur N., ed., Allen's Astrophysical Quantities, 4th edn. AIP Press, New York, p. 381
Eastman R. G., Schmidt B. P., Kirshner R., 1996, ApJ, 466, 911
Elmhamdi A., Chugai N., Danziger I. J., 2003a, A&A, 404, 1077
Elmhamdi A. et al., 2003b, MNRAS, 338, 939
Evans R., McNaught R. H., 2003, IAU Circ., 8150, 2
Ferguson A. M. N., Gallagher J. S., Wyse R. F. G., 1998, AJ, 116, 673
Freedman W. L. et al., 2001, ApJ, 553, 47
Gal-Yam A., Ofek E. O., Shemmer O., 2002, MNRAS, 332, L73
Garnavich P., Bass E., 2003, IAU Circ., 8150, 3
Hamuy M., 2001, PhD thesis, Univ. Arizona
Hamuy M., 2003, ApJ, 582, 905
Hamuy M., 2004a, in Freedman W. L., ed., Carnegie Obs. Astrophys. Ser. Vol. 2, Measuring and Modeling the Universe. Carnegie Observatories, Pasadena, http://www.ociw.edu/ociw/symposia/series/symposium2/proceedings.html
Hamuy M., 2004b, in Marcaide J. M., Weiler K. W., eds, Cosmic Explosions. On the 10th Anniversary of SN1993J (IAU Colloquium 192). Springer, Heidelberg, p. 535
Hamuy M., Pinto P. A., 2002, ApJL, 566, L63
Hamuy M. et al., 2001, ApJ, 558, 615
Heger A., Fryer C. L., Woosley S. E., Langer N., Hartmann D. H., 2003, ApJ, 591, 288
Henden A., 2002, GRB Circular Network, 1242, 1
Holtzman J. A., Burrows C. J., Casertano S., Hester J. J., Trauger J. T., Watson A. M., Worthey G., 1995, PASP, 107, 1065
Howarth I. D., Murray J., Mills D., Berry D. S., 2003, Starlink User Note 50.24
Irwin M., Lewis J., 2001, New Astron. Rev., 45, 105
Karachentsev I. D., Tikhonov N. A., 1994, A&A, 286, 718
Kotak R., Meikle W. P. S., Smartt S. J., Benn C., 2003, IAU Circ., 8152, 1
Kowal C. T., 1968, AJ, 73, 1021
Leonard D. C. et al., 2002a, PASP, 114, 35
Leonard D. C. et al., 2002b, AJ, 124, 2490
Leonard D. C., Kanbur S. M., Ngeow C. C., Tanvir N. R., 2003, ApJ, 594, 247
Mazzali P. A. et al., 2002, ApJL, 572, L61

Nadyozhin D. K., 2003, MNRAS, 346, 97
Pastorello A., 2003, PhD thesis, Univ. Studi di Padova
Pastorello A., Ramina M., Zampieri L., Navasardyan H., Salvo M., Fiaschi M., 2004a, in Marcaide J. M., Weiler K. W., eds, Cosmic Explosions. On the 10th Anniversary of SN1993J (IAU Colloquium 192). Springer, Heidelberg, p. 195
Pastorello A. et al., 2004b, MNRAS, 347, 74
Perlmutter S. et al., 1999, ApJ, 517, 565
Pierce M. J., 1994, ApJ, 430, 53
Piotto G., Capaccioli M., Bresolin F., 1992, Mem. Soc. Astron. Italiana, 63, 465
Riess A. G. et al., 1999, AJ, 117, 707
Rigon L. et al., 2003, MNRAS, 340, 191
Rozanski R., Rowan-Robinson M., 1994, MNRAS, 271, 530
Schlegel D. J., Finkbeiner D. P., Davis M., 1998, ApJ, 500, 525
Sharina M. E., Karachentsev I. D., Tikhonov N. A., 1996, A&AS, 119, 499
Shostak G. S., van der Kruit P. C., 1984, A&A, 132, 20
Smartt S. J., Gilmore G. F., Tout C. A., Hodgkin S. T., 2002a, ApJ, 565, 1089
Smartt S. J., Vreeswijk P. M., Ramirez-Ruiz E., Gilmore G. F., Meikle W. P. S., Ferguson A. M. N., Knapen J. H., 2002b, ApJL, 572, L147
Smartt S. J., Maund J. R., Gilmore G. F., Tout C. A., Kilkenny D., Benetti S., 2003a, MNRAS, 343, 735
Smartt S. J., Maund J. R., Hendry M. A., Benn C. R., 2003b, IAU Circ., 8152, 4
Smartt S. J., Maund J. R., Hendry M. A., Tout C. A., Gilmore G. F., Mattila S., Benn C. R., 2004, Sci, 303, 499
Sohn Y., Davidge T. J., 1996, AJ, 111, 2280
Sohn Y., Davidge T. J., 1998, AJ, 115, 130
Stetson P. B., 1987, PASP, 99, 191
Stetson P. B., Harris W. E., 1988, AJ, 96, 909
Theureau G., Bottinelli L., Coudreau-Durand N., Gouguenheim L., Hallet N., Loulergue M., Paturel G., Teerikorpi P., 1998, A&AS, 130, 333
Tonry J. L., Blakeslee J. P., Ajhar E. A., Dressler A., 2000, ApJ, 530, 625
Tonry J. L. et al., 2003, ApJ, 594, 1
Tully R. B., 1988, Nearby galaxies catalog. Cambridge Univ. Press, Cambridge and New York, p. 221
Turatto M. et al., 1998, ApJL, 498, L129
Van Dyk S. D., Li W., Filippenko A. V., 2003, PASP, 115, 1289
de Vaucouleurs G., 1979, ApJ, 227, 729
Zampieri L., Pastorello A., Turatto M., Cappellaro E., Benetti S., Altavilla G., Mazzali P., Hamuy M., 2003, MNRAS, 338, 711
Zampieri L., Ramina M., Pastorello A., 2004, in Marcaide J. M., Weiler K. W., eds, Cosmic Explosions. On the 10th Anniversary of SN1993J (IAU Colloquium 192). Springer, Heidelberg, p. 275

This paper has been typeset from a TEX/LATEX file prepared by the author.